

Photometric and Spectroscopic Studies of Massive Binaries in the Large Magellanic Cloud. I. Introduction and Orbits for Two Detached Systems: Evidence for a Mass Discrepancy?¹

Philip Massey², Nidia I. Morrell³, Kathryn F. Neugent², Laura R. Penny⁴, Kathleen DeGioia-Eastwood⁵, and Douglas R. Gies⁶

ABSTRACT

The stellar mass-luminosity relation is poorly constrained by observations for high mass stars. We describe our program to find eclipsing massive binaries in the Magellanic Clouds using photometry of regions rich in massive stars, and our spectroscopic follow-up to obtain radial velocities and orbits. Our photometric campaign identified 48 early-type periodic variables, of which only 15 (31%) were found as part of the microlensing surveys. Spectroscopy is now complete for 17 of these systems, and in this paper we present analysis of the first two, LMC 172231 and ST2-28, simple detached systems of late-type O dwarfs of relatively modest masses. Our orbit analysis yields very precise masses ($\sim 2\%$), and we use tomography to separate the components and determine effective temperatures by model fitting, necessary for determining accurate (0.05-0.07 dex) bolometric luminosities in combination with the light-curve analysis. Our approach allows

¹This paper includes data gathered with the 6.5 meter Magellan and 1.0 meter Swope Telescopes located at Las Campanas Observatory, Chile, as well as data obtained with the SMARTS Consortium 1.3 and 1.0 meter telescopes located at Cerro Tololo Inter-American Observatory, Chile.

²Lowell Observatory, 1400 W. Mars Hill Road, Flagstaff, AZ 86001, USA; phil.massey@lowell.edu; kneugent@lowell.edu

³Las Campanas Observatory, Carnegie Observatories, Casilla 601, La Serena, Chile; nmorrell@lco.cl

⁴Department of Physics and Astronomy, The College of Charleston, Charleston, SC 29424, USA; pennyl@cofc.edu

⁵Department of Physics and Astronomy, Northern Arizona University, P.O. Box 6010; Flagstaff, AZ 86011-6010; kathy.eastwood@nau.edu

⁶Center for High Angular Resolution Astronomy and Department of Physics and Astronomy, Georgia State University, P.O. Box 4106, Atlanta, GA 30302, USA; gies@chara.gsu.edu

more precise comparisons with evolutionary theory than previously possible. To our considerable surprise, we find a small, but significant, systematic discrepancy: all of the stars are slightly under-massive, by typically 11% (or over-luminous by 0.2 dex) compared to that predicted by the evolutionary models. We examine our approach for systematic problems, but find no satisfactory explanation. The discrepancy is in the same sense as the long-discussed and elusive discrepancy between the masses measured from stellar atmosphere analysis with the stellar evolutionary models, and might suggest that either increased rotation or convective overshooting is needed in the models. Additional systems will be discussed in future papers of this series, and will hopefully confirm or refute this trend.

Subject headings: binaries: eclipsing — binaries: spectroscopic — stars: early-type — stars: fundamental properties

1. Introduction

1.1. Motivation

The mass of a star is arguably its most fundamental quantity; according to the Russell-Vogt theorem, it is the mass of a star (along with the chemical composition) that uniquely determines a star’s evolution. We now know that the initial angular momentum also plays an important role in determining the evolution of a star (Maeder & Meynet 2000; Meynet & Maeder 2000).

For most stars, the simple way to estimate the mass (m) of a star is by measuring the star’s luminosity (L), as $L \sim m^x$ where the exponent x is approximately 4 for solar-type stars. For both lower mass ($< 0.5M_{\odot}$) and higher mass ($> 10M_{\odot}$) stars, the exponent becomes smaller, due to the importance of convection in lower mass stars, and radiation pressure in higher mass stars. For most stars, the exponent in this mass-luminosity relationship (MLR) is well established both by evolutionary theory and empirical measurements¹.

However, for high mass stars there are two additional complications that make applying the MLR difficult. First, main-sequence massive stars (O- and early B-type) stars are quite hot ($T_{\text{eff}}=25,000\text{-}50,000$ K) and because of this only a tiny fraction of their light leaks out in the visible. In order to apply the MLR, one needs to know not only the distance and

¹Indeed, one of the great vindications of stellar evolutionary theory was the fact that Eddington (1924) was able to derive the exponent for solar-type stars purely from the physics of radiative diffusion.

reddening of a star (in order to get the absolute visual magnitude, M_V), but also an accurate value for the effective temperature, as the correction to M_V needed to obtain the bolometric luminosity is a steep function of effective temperature. The second complication is that the MLR is really a function of age. This is true for all stars, as their luminosities increase slightly as they evolve, but massive stars also *lose mass* as they evolve, due to radiatively-driven stellar winds. For massive stars these issues can be solved by first modeling the optical spectra using non-LTE stellar atmosphere codes, such as CMFGEN (Hillier & Miller 1998) or FASTWIND (Puls et al. 2005). This then provides both the effective temperature and the bolometric luminosity, allowing placement of the stars on the H-R diagram (HRD). Reference to stellar evolutionary models then allow a determination of age and current mass (referred to often as the “evolutionary mass”) without reference to a MLR *per se*.

However, this method is no better than the stellar atmosphere and evolutionary models on which they are based. A worrisome issue that remains is that of the so-called “mass discrepancy”, a systematic difference between the masses one obtains from a stellar atmosphere analysis, and that inferred from evolutionary theory. Modeling the star’s spectra with a stellar atmosphere code produces a measurement of the mass via the surface gravity g , since $g \sim m/R^2$, and the radius R is known once the effective temperature is known *if* the distance and hence the luminosity L are known, since $R^2 \sim L/T_{\text{eff}}^4$ by the Stefan-Boltzmann equation. Herrero et al. (1992) called attention to the fact that the masses derived from spectroscopic analysis are systematically lower than those found from evolutionary models. This mass discrepancy has never been fully resolved, despite significant improvements in both the evolution and stellar atmosphere models. (See, for example, Massey et al. 2005.) But it would be of great interest to measure masses in some more direct way to test the validity of the models. Such an opportunity is granted to us by binaries, where Newtonian physics and Kepler’s 3rd law provides us (in principle) with direct mass measurements.

This is the first of a series of papers presenting dynamical masses and bolometric luminosities for massive stars in the Large Magellanic Cloud (LMC). The title of our series is intended to pay homage to the “Spectroscopic Studies of O-type Binaries” series by Peter S. Conti and collaborators, which appeared 30-35 years ago (e.g., Bohannon & Conti 1976; Conti & Walborn 1976; Massey & Conti 1977; Morrison & Conti 1978, 1980; Conti et al. 1980). Although telescopes have gotten larger since those days, and instruments and data analysis methods have improved, the basic need to test theory with fundamental mass determinations remains. Work over the past several decades has helped improve the situation² but the paucity of systems with well-determined parameters is underscored by our continuing

²We particularly want to acknowledge the many contributions in the field by our late friend and colleague Virpi Niemela.

poor knowledge of the MLR and the persistence of the mass discrepancy.

1.2. Our Approach

Historically, studies of massive binaries have usually begun by the accidental discovery of double lines in the spectrum as a result of an observation taken when the system just happened to be near orbital quadrature³. Several dozen subsequent spectra are then usually needed (obtained over a period of months or years) to determine the orbital period and the orbital parameters. Usually it is only then that the system is monitored to detect the light variations that would indicate eclipses that allow an orbital inclination (i) to be determined. Without knowledge of the inclination, a double-lined spectroscopic orbit solution tells us only the *minimum* masses for each component, $m_1 \sin^3 i$ and $m_2 \sin^3 i$, since $\sin^3 i \leq 1$.

If eclipses are present, then analysis of the light curve will also yield the stellar radii and the flux ratios of the two components, if the effective temperatures can be accurately determined. For most stars the effective temperatures can be determined by obtaining light curves in different bandpasses (i.e., from the colors), but for main-sequence massive stars, the colors are largely degenerate with effective temperatures because of the high temperatures, and it requires additional spectral analysis if good values for the effective temperatures are to be found. With these, and with the knowledge of stellar radii, one can then compute the bolometric luminosities of the components, which can be used to refine our knowledge of the mass-luminosity relationship. It is additionally useful to know the distances to the system, as the comparison between the modeled absolute visual magnitude and the observed absolute visual magnitudes provides assurance that the physical parameters are correct⁴.

Since eclipsing systems are necessary for the full analysis, we decided to instead start by searching for stars whose light curves suggested they might be eclipsing massive stars. We chose to concentrate on massive stars in the Magellanic Clouds since their distances are well known, and they are bright enough for spectroscopic followup, albeit with larger

³Throughout this paper we refer to the phases where eclipses occur (conjunction) as phases 0 and 0.5, and to the phases that are most double-lined (quadrature) as phases 0.25 and 0.75.

⁴We note that the courageous efforts of several groups who invert this problem in order to determine distances to nearby galaxies by measuring the stellar radii from the eclipses and orbital parameters, and then using the effective temperatures to infer the absolute magnitude of the system, which can then be compared to observed magnitude to derive a distance. See, for example, the review by Paczynski (1997), and recent work by Bonanos et al. (2006, 2011), Guinan et al. (1998); Harries et al. (2003), Hilditch et al. (2005), Fitzpatrick et al. (2003), North et al. (2010), and Vilardell et al. (2010), to name but a few such attempts.

apertures. In addition, since their metallicities are relatively low, mass loss on the main-sequence should be relatively modest, and thus the connection to the initial masses should be less dependent upon the assumed mass loss rates of the evolutionary models. By refining the periods and times of primary eclipses precisely using frequent photometric observations prior to spectroscopic observations, we should know exactly when to observe these stars at maximum velocity separation (orbital quadrature).

This allowed us to measure the orbital semi-amplitudes very efficiently for two reasons. First, O-type stars have very broad spectral lines due to rotational broadening ($v \sin i$ typically greater than 100 km s^{-1}), and *most* spectral observations more than 0.1 phase away from quadrature are unlikely to show resolvable double lines and hence do not provide useful measurements. Secondly, it is the velocities around quadrature that best define the orbital semi-amplitudes. And, since the phases would be known exactly, determining the amplitude of the orbital motion could be done with very few observations, as we could fix the phases in the orbital solutions to those determined from the light curve. Thus we minimized the amount of large telescope time needed for the spectroscopy by utilizing small aperture telescopes to determine the light curves⁵.

One of the downsides to this approach is that it is easier to find short period systems as their light variabilities are more pronounced: for a given orbital inclination eclipses will be deeper for shorter period systems. However, these shorter period systems are more likely to be in contact, and therefore their masses will be less pertinent to understanding single stars. But for many such systems our program detected easily interpreted, detached systems. Nevertheless, as we will see, even these “simple” systems offer some unexpected surprises!

We begin this series of papers with a study of two such simple, detached system consisting of late O-type dwarfs of modest mass: [M2002] LMC 172231 (O9 V + O9.5 V) and ST2-28 (O7 V + O8 V). Subsequent papers will describe the other eclipsing systems we’ve identified, including early-type O binaries, Wolf-Rayet binaries, and contact systems. We describe in some detail here the observational and reduction techniques, since these will be used in this future work, and illustrate the results we’ve been able to achieve. It is our intent that these systems will allow us to make more critical tests of stellar evolution models than usually possible, and to serve as *linchpins* for the empirical mass-luminosity relationship.

⁵Some studies, such as Gonzalez et al. (2005), Morrell et al. (2007), and Bonanos (2009) have used massive eclipsing binaries found by way of the MACHO (Alcock et al. 1997) and OGLE (Udalski et al. 1998) microlensing searches. Here we decided to obtain our own photometry as the data needed to be nearly contemporaneous with the spectroscopy for precise phases, and also because we suspected such surveys might have missed many interesting systems. Based upon the scant number of our systems that were detected by MACHO and OGLE, as discussed below, our approach appears to have been justified.

2. Observations and Reductions

2.1. Photometry and the Identification of Eclipsing Systems

Our photometric monitoring of stars in selected OB associations in the Magellanic Clouds began in 2003 July, and continued through 2011 February. The observing seasons generally extended from August through January or February of the following year. The only observing season missed entirely in our photometric monitoring program was 2008/2009, as we had begun our spectroscopic observations, but as the analysis proceeded we realized we needed more supporting photometry. The only observations during the 2010/2011 season were made in January-February 2011 of selected stars at targeted times in order to improve missing phase coverage in the light curves.

A variety of telescopes were used; their properties are listed in Table 1. The Swope observations were made in “classical” mode by N.I.M.⁶ and were often nightly during dark time. The SMARTS 1.0-m and 1.3-m observations were obtained in queue mode usually with a cadence of once every other night throughout both bright and dark time, with time primarily allocated through Georgia State University, although the first season was obtained through NOAO (Proposal 2005B-0108). In the case of the 1.0-m, the queue observations were carried out for a few minutes each night by whatever astronomer happened to be scheduled that night in classical mode; in the case of the 1.3-m, the data were obtained by dedicated queue observers. We list in Table 2 the six Magellanic Cloud regions we observed, and which telescopes were used in each observing seasons. This table is intended primarily to give an overall view of the scope of the project; the specific telescope and instrument will be given for each photometric measurement in the individual photometry tables. All observations were made through a V filter, and exposure times were typically 10-30 sec. Data were obtained under both photometric and non-photometric conditions (in some cases, through several magnitudes of extinction!), but since each field contained hundreds of reference stars, we were able to obtain good photometry nonetheless.

The reductions of the Swope data were straightforward. Our tests on a series of exposures did not justify the use of the nonlinearity correction typically applied to these data (Hamuy et al. 2006), but inclusion or not would have had negligible effect on our photometry. Overscan columns were used to remove the bias, and nightly bias frames were used to remove the (negligible) bias structure. Flat fielding was achieved by exposures of dome flats.

The SMARTS 1.0-m Yale Y4KCam data proved a challenge to reduce. Our data were

⁶During the 2005/2006 observing season she was aided by her co-workers in the Carnegie Supernova Project (Hamuy et al. 2006).

among the first to be taken with the instrument, and our reductions quickly identified a number of issues. The $4K \times 4K$ chip was read out using four amplifiers, and we found we had to mask out the central rows and columns as good photometry could not be performed for stars that straddled quadrants as the bias structure was highly unstable. Worse, tests showed that dome flats and twilight sky flats differed by nearly 10% from center to edge. We prevailed upon one of the observers, David James, to obtain images with the star moved from center to near the edge, and our photometry of these data showed that the twilight flats gave good ($<1\%$) results while the use of dome flats would have resulted in a 10% error. The lack of header information describing the data and bias sections of the four quadrants resulted in our writing our own IRAF⁷ reduction scripts, which have been made available on the SMARTS web site⁸ for others to use, along with the characterization of the instrument. We hope this provided some partial compensation for the scheduled observers who were asked to take 15 minutes of data for us every few nights.

At the start of the 2007/2008 observing season, one quadrant of the Y4KCam chip died, and our program was switched to the SMARTS 1.3-m ANDICAM instrument. Reduced data are kindly provided for all ANDICAM observations by Suzanne Tourtellotte, and the reductions are essentially identical to what we used for the Swope data.

Photometry was carried out by a series of automatic IRAF scripts that characterized the data, identified stars, and obtained aperture photometry. These routines were loosely based upon the scripts written for producing photometry for the Local Group Galaxies Survey (Massey et al. 2006, 2007). Experiments to perform photometry via point spread function (PSF) fitting did not yield improved results, and often were inferior, particularly on the SMARTS 1.0-m Yale data where significant PSF variations were present across the field. For the Swope and SMARTS 1.3-m data, an aperture with a radius of 3 pixels was used ($1''.1-1''.3$). For the SMARTS 1.0-m data, a similar value in arcseconds was used (5 pixels, or $1''.4$). The sky values were taken from the modal value in an annulus located between radii of 10 and 18 pixels from each star.

For each telescope and cluster combination a “master list” was created, consisting of pixel coordinates and an instrumental magnitude for each star from some frame obtained in good seeing. In addition, each master list included the celestial coordinates for each star, obtained by using the *HST* Guide Star Catalog 1.1 catalog to calibrate the frame with a

⁷IRAF is distributed by the National Optical Astronomy Observatory, which is operated by the Association of Universities for Research in Astronomy (AURA) under cooperative agreement with the National Science Foundation.

⁸<http://www.astro.yale.edu/smarts/smarts1.0m.html>

world coordinate system. The masterlist also included our best estimate of the standard magnitude of each star, obtained using the UBVRI photometry of Massey (2002) and a modest color correction determined for each telescope from a B image obtained for these purposes. The photometry from each frame was cross-correlated against this master list in order to determine the offset, rotation, and a magnitude difference for the ensemble. The magnitude for each star was then determined by correcting for the magnitude difference of the frame to the masterlist, and the correction between the masterlist’s instrumental magnitude and our estimate of the standard magnitude. A single file of the photometry of each star was then produced including the heliocentric Julian day (HJD) and the magnitude and instrumental magnitude error. The photometry from the various years and telescopes were then combined, applying a small zero point shift (typically on the order of several thousandths of a magnitude) if needed to bring the median out-of-eclipse data into accord.

We analyzed the data as we went along, and re-evaluated our target list every year, with the goal of having a preliminary set of targets for spectroscopy in late 2008. It is for that reason that we dropped NGC 602c from our program (see Table 2), as none of the stars of interest showed significant variability.

Various methods have been employed over the years to detect variability. In our case, we were interested only in *periodic* variability. We therefore adopted the one-way analysis of variance (AOV) method of Schwarzenberg-Czerny (1989) which excels at detecting periodic narrow events, inspired by the success demonstrated by López-Morales & Clemens (2004). (We are grateful to Mercedes López-Morales for helpful correspondence and for passing on a FORTRAN77 version of the Schwarzenberg-Czerny 1989 code. Updated versions of the code can be found at Dr. Schwarzenberg-Czerny’s web site⁹.) We added software that allowed the automatic detection of the spikes in the resulting periodograms, and produced phased light curves that could be examined by eye for significance and to distinguish likely periods from their aliases. In all, several *thousand* such light curves were examined multiple times as the data collection grew; this provided useful training material for a number of undergraduates.

For the final periods, we checked our values using the Lafler & Kinman (1965) technique, which involves phasing the data by successive trial periods and determining the point-to-point scatter in the phased data.

We list in Table 3 *all* 48 of the stars in the SMC and LMC that we thought were interesting from the light curves; follow up spectroscopy (described in the next section) caused us to drop many of these from our program for one reason or another. For some, the stars were not double-lined at the anticipated phase. This is unlikely due to our having the

⁹<http://users.camk.edu.pl/alex/>

wrong period, as in some cases the same period had been found from analysis of MACHO data (Faccioli et al. 2007, Derekas et al. 2007). In other cases, double lines were seen but were too blended for reliable velocity information to be extracted. In a few cases it was just not possible to obtain a sufficient number of observations at the needed orbital phases due to time spent on other systems. In one very disappointing case, that of the early-type binary NGC 346 MPG 342 (Massey et al. 1989), spectroscopy revealed that the system was triple, with the third component also shifting. In the end we were left with no suitable stars in the SMC, and 17 in the LMC.

Wyrzykowski et al. (2004), Derekas et al. (2007), and Faccioli et al. (2007) have published lists of eclipsing binaries in the SMC and LMC from the OGLE (Udalski et al. 1998) and MACHO (Alcock et al. 1997) microlensing projects, and it is interesting to note that of the 48 periodic light variables we found, only 15 (31%) of them are also in these lists. The reasons for this are not obvious. Saturation is likely not the sole explanation: the brightest stars in the Wyrzykowski et al. (2004) and Derekas et al. (2007) catalogs have $V \sim 13$, while the average V magnitude of stars in our sample have $V \sim 14$. Of the two stars discussed in the present paper, the V magnitudes are nearly the same ($V=14.04$ and 14.15), and yet one was previously detected as a variable while the other one was not. None of the stars in NGC 1910 or the R136 region are identified as eclipsing systems by these other studies. R136 is embedded in strong nebulosity, but the nebulosity around NGC 2074 (where numerous MACHO objects are found) is considerably stronger than that of NGC 1910. Crowding may also be an issue, although one of the stars discussed in the current paper (ST2-28) is relatively crowded and was correctly identified. It is also true that in some cases the periodic variability was of very low amplitude. For instance, LMC 171520, which will be discussed in Paper II, has peak-to-trough variations of <0.1 mag. Still, other stars, such as one of the stars discussed in this paper, LMC 172231, have very deep (0.6 mag) eclipses but were not detected in these microlensing surveys. (It is also not located in strong nebulosity.) We believe this emphasizes the need for such targeted studies such as ours, particularly for finding massive eclipsing systems where nebulosity is a characteristic of the sample.

We do note that when MACHO or OGLE did detect our objects, the periods are in excellent agreement. The one exception is LMC 164717, where the MACHO period is half of ours.

2.2. Spectroscopy and Radial Velocities

All spectroscopy intended for radial velocities was carried out on the Magellan Clay and Baade 6.5-m telescopes, although a few classification spectra were also obtained on the

DuPont 2.5-m telescope. The large aperture of the Magellan telescopes allowed us to reach the very high signal-to-noise (S/N) we desired (200 or more per 1 \AA spectral resolution element) in exposures of about an hour for our faintest targets, and a few minutes for our brightest. Such high S/N is needed given the general weakness of the spectral features in early-type stars.

All in all, we collected data at the Magellan telescopes on 21 nights between 2008 December 8 and 2010 November 27. The individual runs varied in length from 2 to 6 consecutive nights. Roughly half of the time was allocated through Carnegie, and the other half through the University of Arizona. Nine of the nights were on the Baade with the Inamori-Magellan Areal Camera and Spectrograph (IMACS), while the other 12 nights were on the Clay telescope with the Magellan Echellette (MagE) spectrograph. Generally, the first three authors (P. M., N. I. M., and K. F. N.) were present for all of the observing, although for a few runs either P. M. or N. I. M. were the only ones observing.

For all of the observing, orbital ephemerides were computed based upon the accumulated photometry prior to the observing run, and observations were planned to take place near orbital phases of 0.25 and 0.75, the times of maximum velocity separations. Quick-look was performed in real time to assess the overall quality of the data, and (in the first few spectroscopic runs) to determine spectral types and confirm that double lines were present.

For IMACS, observations were obtained with the $1200 \text{ line mm}^{-1}$ grating with a $0''.9$ slit. The resulting spectral resolution was about 1.0 \AA (5.0 pixels on the detector). Spectral coverage was nominally $3650\text{-}5250 \text{ \AA}$ over the four CCDs, but in practice only the central two chips contained useful spectral features and were used, covering $4020\text{-}4410 \text{ \AA}$ and $4430\text{-}4820 \text{ \AA}$. Because IMACS uses a very long slit, it was often possible to rotate the instrument to a position angle that allowed two objects of interest to be placed on the slit and observed at the same time. A series of three integrations (ranging from $3 \times 300 \text{ s}$ to $3 \times 750 \text{ s}$ depending upon the brightness of the object and the sky conditions) was obtained of the program object, followed by a 150 s exposure for the HeNeAr. The observing procedure for such spectroscopy is relatively straight forward but time consuming for a program such as ours, as there is no provision for viewing the slit directly. Despite our experience, it was never possible to lower the overhead (setup plus comparison) to less than 10 minutes for each new object. Flat field data were obtained by exposure of a calibration screen during the afternoon. Typical signal-to-noise was 150-200 per 5 pixel resolution element.

Data reduction for IMACS used the standard IRAF tasks. The overscan at the top of each chip was used, as this removed most of the bias structure. The remainder was removed using a series of bias exposures obtained each night. Flat-fielding was accomplished by the normalized calibration screen exposures. Spectra of the sources were extracted using an

optimal extraction “clean” algorithm, with sky chosen adjacent to the object, and combined at the end. Each of the two chips were treated separately. Typical wavelength errors (root mean square) from fitting the comparison spectra were 0.03-0.05 Å (2-3 km s⁻¹).

For MagE, spectral coverage is nominally from 3100 Å to 1μm covering 15 orders, with a spectral resolution of 4100, almost identical to the resolution we achieved with IMACS. We did not reduce either the bluest or reddest parts of the spectra, but kept only the central 13 orders (orders 7-19), covering 3150-9400 Å. Acquisition is by means of a slit-viewing TV, so overhead was minimal. Although the short slit (10”) precluded multiplexing by obtaining two objects, the high throughput and lack of overhead made this a more efficient instrument for our program. Exposure times were shorter than with IMACS by about 30%, and resulted in higher signal-to-noise than with IMACS. Wavelength calibration was by means of a 3 s ThAr exposure.

Flat-fielding of MagE is complicated by the very large wavelength coverage. Traditionally users have employed a combination of flat-field quartz lamp exposures in the red and in- and out-of-focus exposures of a Xe lamp in the violet. Following a suggestion made one night at dinner by Ian Thompson, we experimented and demonstrated to our satisfaction that we could meet our very high signal-to-noise requirement *without* flat fielding: that the chip really is quite uniform. Instead, we dithered the star to three positions along the slit. In the end we typically achieved a S/N of 400 per 4-pixel spectral resolution element at 5000 Å¹⁰.

The reductions of the MagE data were complicated by the curvatures of each order (due to the anamorphic distortions of the cross-dispersing prisms), and spectral features are also tilted, with a tilt that varies with wavelength along each order. Although various MagE pipelines have been developed by several groups, we found we did very well with the “mtools” IRAF package written by Jack Baldwin for dealing with data from another instrument, the Magellan Inamori Kyocera Echelle (MIKE)¹¹, in combination with the standard IRAF Echelle reduction tools. Wavelength calibration consisted of a 2-dimensional fit to all of the orders, with RMS residuals of 0.05-0.06 Å (3-4 km s⁻¹).

Radial velocities were measured from the normalized spectra using interactive fitting of two Gaussians to resolve double lines, a standard technique with double-lined O-type binaries (see, for example, Burkholder et al. 1997, Rauw et al. 2001, Massey et al. 2002, Morrell et

¹⁰We note that many users require significantly lower S/N than ours, sometimes in the single digits. Flat-fielding is unlikely to help such data. See discussion in Massey & Hanson (2012).

¹¹<http://www.lco.cl/telescopes-information/magellan/instruments/mike/iraf-tools>

al. 2003, Niemela et al. 2006, and Mayer et al. 2008)¹². If a spectrum did not reveal double lines, it was not used; an inspection of the data revealed that there were no instances for our final sample where a star should have shown double lines at an appropriate phase but did not, or vice versa, giving us additional confidence in our period determinations. Anywhere from 1 to 17 lines were measured in a given spectrum (mainly the He I and He II although occasionally the Balmer lines were used if well separated) depending upon the phase and the quality of the data, but the typical (median) number was 5. The effective rest wavelengths were taken primarily from Conti et al. (1977), supplemented by the updated version of Moore (1972) by Coluzzi (1993).

3. Analysis: Derivation of Orbital Parameters and Physical Parameters

3.1. Determining the orbital semi-amplitudes and the minimum masses

Typically one uses the radial velocities of each component of a spectroscopic binary to solve for the orbital elements P (the period), K_1 and K_2 (the orbital semi-amplitudes), γ (the center-of-mass motion of the system), T (the time of periastron passage of the primary), e (the orbital eccentricity), and ω (the angular distance of periastron passage relative to the ascending node). In general the radial velocity v_1 of star 1 is related to the orbital parameters as

$$v_1 = \gamma + K_1 e \cos \omega + K_1 \cos(\nu + \omega),$$

where ν is the true anomaly, a function only of the orbital phase and e (see, e.g., equations 64 and 65 in Binnendijk 1960). The minimum masses are given by

$$m_1 \sin^3 i = 1.036 \times 10^{-7} (K_1 + K_2)^2 K_2 P (1 - e^2)^{3/2} \quad (1)$$

and

$$m_2 \sin^3 i = 1.036 \times 10^{-7} (K_1 + K_2)^2 K_1 P (1 - e^2)^{3/2} \quad (2)$$

when P is expressed in days, K in km s^{-1} , and m is in solar masses. The orbital inclination relative to the line of sight is i , and hence the expression *minimum* mass, as $\sin^3 i \leq 1$. Note from these equations that mass ratio is inversely proportional to the ratio of the semi-amplitudes; i.e., $m_2/m_1 = K_1/K_2$.

In designing our spectroscopic observations, we decided to concentrate on the systems with circular orbits, as one can then eliminate the need to determine e and ω , and fewer

¹²The scant number of spectral lines in the spectrum of O stars means that standard cross-correlation techniques are less useful than for stars of later spectral types.

observations will yield high accuracy for the orbital semi-amplitudes and hence the masses. Fortunately, we expect that to be the case for most massive binaries with short periods, as tidal forces circularize orbits very quickly. (For instance, of the 15 young detached massive binary systems listed by Gies 2003 with periods less than 5 days, only 2, or possibly 3, have been shown to have non circular orbits.) For eclipsing systems, most systems with non-circular orbits can be quickly spotted as the primary and secondary eclipses will likely be separated by other than 0.5 phase. However, an eccentric system which just happens to have ω near 90° or 270° will also have eclipses 0.5 phase apart, and so the definitive test will come from modeling the light curve. An light curve with eclipses 0.5 phase apart *and* the same eclipse widths means that the orbit is circular.

For massive binaries there can be a further complication. Hot luminous stars have radiatively-driven stellar winds that, if strong enough, may result in appreciable (tens of km s^{-1}) outward motion even down in the photosphere where the spectral lines are formed. This was first demonstrated in a series of papers by Hutchings (1968a, 1968b, 1969, 1970a, 1970b; see also 1979). This results in the possibility that the two components in an early-type binary may have different average velocities, equivalent to saying that separate “center of mass” velocities may be needed for each component, i.e., that actually γ_1 and γ_2 are needed. Examples include the Of-type binaries HDE 228766 (Massey & Conti 1977, Rauw et al. 2002) and Sk-67° 105 (Niemela & Morrell 1986) where the “systemic” velocities of the two components differ by 30-40 km s^{-1} or more. In many cases, however, the γ velocities agree within the errors, particularly if the components are late O-type dwarfs (see, for example, Stickland et al. 1997, Penny et al. 2002) as these stars will have weaker stellar winds than early O stars or Of-type supergiants. This issue sometimes comes as a surprise even to binary experts used to working on less massive stars, or is overlooked by newcomers to the field¹³.

In order to minimize the amount of spectroscopy time needed, and to put all of the radial velocity information towards the most accurate determinations of the orbital semi-amplitudes, we adopt the values of T and P from the light curve in order to compute the phase θ . Then for circular orbits ($e = 0.00$) the relationship between the observed radial velocities v and the orbital parameters K and γ become simple linear equations,

$$v_1 = -K_1 \sin 2\pi\theta + \gamma_1 \tag{3}$$

$$v_2 = K_2 \sin 2\pi\theta + \gamma_2, \tag{4}$$

¹³Some hesitancy to accept the occasional need for two different values of γ may trace back to the realization by Petrie (1962) that poorly determined values for e and ω will result primarily in erroneous values for γ ; see discussion in Batten (1973).

where θ is the fractional part of $(t - T)/P$, where t is the heliocentric Julian day (HJD) of the observation, and T is the HJD corresponding to primary conjunction, when the secondary is in front of the primary. Thus one can compute the values for the K 's (and hence the masses) much more precisely than in cases where the radial velocities are also used to determine P and T and hence θ .

In practice, we solved Equations 3 and 4 both with the individual γ 's and with a single γ (i.e., $\gamma_1 = \gamma_2 = \gamma$), and compared the residuals. In only a few cases did we find that using individual values for γ were warranted. (Both of the systems discussed here were well modeled with a single γ , consistent with their being late O-type dwarfs, presumably with small mass loss-rates.) We determined the best values for the K 's and γ by least-square fitting, we assigned $1/\sigma_\mu^2$ weight to each velocity, where σ_μ is the standard deviation of the mean for each velocity. If only one spectral line was measured, we assumed a large velocity error (30 km s^{-1}) so as to include the point but with low weight. If σ_μ was less than 5 km s^{-1} we assumed the actual error was 5 km s^{-1} , so as not to overweight points where the few individual velocities forming the average were fortuitously similar. We also ran a differential orbit fitting program (written by our colleague L. H. Wasserman and described in more detail by Rosero et al. 2011) on the velocity data to confirm that the data were consistent with our assumption of a circular orbit.

A nearly independent check on our orbital semi-amplitudes is provided by the method of Wilson (1941), who demonstrated that one could determine the ratios of the orbital semi-amplitudes directly from the radial velocities themselves without knowledge of the period or indeed any of the orbital parameters. It is applicable for non-circular (as well as circular) orbits. (In practice, this works reliably only if there are velocity measurements from both sides of the orbit.) If one plots the radial velocity v_2 against v_1 , the slope of the best fit line will be proportional to the ratio of the orbital semi-amplitudes, $\Delta v_2/\Delta v_1 = -K_2/K_1$, which is just the negative of the inverse mass ratio $-m_1/m_2$.

The intercept is $\gamma(1 + K_2/K_1)$. Massey & Conti (1977) showed that, in the case that two different γ 's were needed, the slope remains the same, but the meaning of the intercept changes to be $\gamma_2 + \gamma_1(K_2/K_1)$. “Wilson’s method” was used by Bohannan & Conti (1976) and Massey & Conti (1977) in their studies of high mass systems, and has been employed to good effect recently by Lisa Prato and collaborators (e.g., Prato 2007, Schaefer et al. 2008, Mace et al. 2009, Rosero et al. 2011) in their studies of low-mass binaries. The resulting mass ratios and the linear correlation coefficients r from the Wilson diagrams are included in describing our orbit solutions.

The improvement in computer processing power and analytical techniques have made it possible to solve for both light- and radial velocity curves simultaneously; these sophisticated

programs model the “center of light” velocities, which are no longer the simple sine curves given in Equations 3 and 4 near conjunction if the systems eclipse, or if tidal distortions are significant. In the cases we consider here, the stars are nearly perfectly round (as discussed in Section 4), and none of our velocity measurements are taken near conjunction. Indeed, for massive O-type stars, with their broad spectral lines, double lines can only be resolved near quadrature and so the use of these advanced tools of are limited benefit.

3.2. Determining the orbital inclinations and other physical components

Our light curves combined with the orbital parameters allow us to determine the orbital inclination, and they also allow us to determine the individual flux ratios between the two stars by adopting effective temperatures. From first principles we expect that (in the absence of tidal distortions and the like) the same areas will be eclipsed at both primary and secondary eclipse. Thus, the deeper eclipse will correspond to the hotter star being eclipsed as the surface brightness of the hotter star will be greater (at every wavelength) according to the Stefan-Boltzmann law. However, this is not necessarily the *brighter* star, nor is it necessarily the star with the stronger spectral features.

Consider this from the standpoint of stellar evolution. A binary might form consisting of two stars with nearly equal masses. The slightly more massive one will be the hotter one, initially. It will also have a slightly larger radius and bolometric luminosity. It will also be the brighter one visually. It will also be losing mass at a slightly higher rate (through radiatively driven stellar winds) than its companion. However, as stellar evolution proceeds its temperature will decrease. Most stellar evolutionary models would have its bolometric luminosity increasing as well. So, in the absence of complications it should remain the visually brighter star. However, because of mass-loss, it may not remain the more massive of the two components. Thus a system that begins as an O5 V + O6 V pair (with the O5 V star the more massive component) could evolve to an O7 III + O6.5 V pair, but either component could be the more massive. In such a system the light curve would show the deepest eclipse when the O6.5 V component was eclipsed, since it would be the hotter star. We’ll note that because the luminosity class “V” is very broad in terms of its spectral features, the O5 V + O6 V pair could even be classified as O7 V+O6 V at a later time. It is not clear which component would be the more massive given the fact that both stars will be losing mass, with the initially more luminous (massive) star having the larger mass-loss rate. Thus we should not expect that the hotter component (which we will call the primary) is necessarily the more massive component.

For modeling the eclipses, we used the light curve synthesis code GENSYN (Mochnacki

& Doughty 1972) to produce model V -band differential light curves. Our approach was to make a constrained fit using as much data as possible from the spectroscopic results. The orbital parameters were taken from the spectroscopic solution, and initial effective temperatures were estimated from the spectral types of the stars, using the calibrations of Massey et al. (2005) and Trundle et al. (2007) for O-type and B-type stars, respectively. We then estimated the physical fluxes and limb darkening coefficients from tables in the OSTAR2002 and BSTAR2006 models¹⁴ based upon TLUSTY (Hubeny & Lanz 1995), and Claret (2000), respectively. Each trial run of GENSYN was set by three independent parameters, the system inclination i and primary and secondary polar radii. For the initial run, we attempt to match three observables: the absolute visual magnitude of the system, the eclipse depths, and the eclipse durations (widths)¹⁵.

We used the velocity curves and the flux ratios to separate the spectra of the two stars using tomographic analysis (Bagnuolo & Gies 1991, 1992; Gies 2004). With these cleanly separated spectra, we next used the stellar atmosphere code FASTWIND (Puls et al. 2005) to model the components, producing more accurate effective temperatures. Examination of the line depths, particularly of the Balmer lines, also allowed us to reevaluate the flux ratios. The new values of the effective temperatures were then used to remodel the light curve. As described below, the star ST2-28 turned out to be triple, with the third component stationary. It was easy to extend our analysis to include this situation.

To briefly summarize, we used the spectroscopic orbit to fix as many of the physical properties of the system as possible, such as the orbital separation. Our preliminary light curve analysis then used a reasonable approximation for the effective temperatures based on the spectral types, and produced a flux ratio. We used this flux ratio to separate the spectra using tomographic analysis, which we then modeled with FASTWIND, yielding improved effective temperatures, and revealed any problem in the flux ratios, which we then used to remodel the light curve. If needed, a new tomographic extraction and remodeling was then performed. This complete an approach has not generally been used on massive binaries, although Fitzpatrick et al. (2003), Bonanos (2009) and Bonanos et al. (2011) did similar fitting using model atmospheres on tomographically separated spectra to determine the effective temperatures. The values of the orbital inclinations were not much affected by this approach, as the value we derived from the final light curve analysis was always within one or two sigma of the original analysis. Rather, the strength of this approach was that it

¹⁴From <http://nova.astro.umd.edu/Tlusty2002/tlusty-frames-guides.html>

¹⁵Note that although the polar radii were entered, the program also reports the “volume radius”, i.e., the radius for a sphere of the same volume as the tidally distorted star. It is this volume radius that we will report, and use with the effective temperatures to determine a bolometric luminosity.

resulted in far more accurate luminosity determinations than could have been achieved by simply trying to match the absolute magnitude of the total system, as the latter is always uncertain by 0.3 mag or so due to uncertainties in reddening, etc.

The bolometric luminosities were computed using the effective temperatures and effective stellar radii in the Stefan-Boltzmann equation. We then found the absolute visual magnitude by subtracting the bolometric correction:

$$\text{BC} = -6.90 \log T_{\text{eff}} + 27.99,$$

from Massey et al. (2005). All this assumes spherical geometry. The light-curve analysis program also produces an estimate of the absolute visual luminosity; this integrates over the (non-spherical) surface, but relies upon inputting the monochromatic specific intensity from the stellar atmospheric models. We feel this method is less certain, but will include it as the “tidal model”, although as we will see, these stars are not much distorted from spheres. The tidal model bolometric luminosity is then found by adding the bolometric correction.

4. Results for Two Detached Systems

The two systems whose orbit solutions and masses we present here were chosen in part because their parameters were very well determined. Higher mass systems, and more physically complex interpretations, will be presented in future papers. Throughout we assume a distance modulus to the LMC of 18.50 (50 kpc), following van den Bergh (2000).

4.1. [M2002]LMC 172231, O9 V + O9.5 V

LMC 172231 is located in a relatively uncrowded region of NGC 2074, also known as the Lucke-Hodge 101 OB association (Lucke & Hodge 1970). The star was first cataloged by Westerlund (1961) in his photographic study of NGC 2074 ([W61] 3-9), and was included in Testor & Niemela (1998)’s photometric and spectroscopic study of the region ([ST92] 5-67)¹⁶. Additional photometry was obtained by Massey (2002) in his survey of the SMC and LMC ([M2002] LMC 172231).

LMC 172231 attracted our attention for its relatively long period (3.225414 days) and a light curve that was characteristic of a detached system (Figure 1). A summary of the

¹⁶The designation [ST92]5-67 is apparently an extension from Zones 1-4 photometered by Schild & Testor (1992).

photometric data can be found in Table 4, and the photometry itself can be found in Table 5. Note from Figure 1 the very good agreement between the photometry from various telescopes and instruments.

Spectroscopy revealed nicely separated double lines, characteristic of two late O-type dwarfs. We show an example of the star’s spectrum at a double-lined phase in Figure 2 *left*. We initially classified the components as O8.5 V and O9 V, although the spectra separated by tomography yield slightly later spectral types than the blended spectra indicated, as described below. Radial velocities were measured primarily from He I and He II, although in a few cases some of the Balmer lines were also used. The radial velocities are given in Table 6, along with the standard deviations of the means, and number of lines measured.

The stars are roughly equally bright; the differences apparent in the spectra (Figure 2) are primarily due to slight differences in spectral type (effective temperature) rather than luminosity. We will refer to the hotter star as the “primary”, keeping with the standard convention.

4.1.1. *Physical Parameters*

If we allow the orbital eccentricity to be a free parameter, holding only the period fixed, we find $e = 0.000 \pm 0.032$, consistent with our expectation from the light curve that the orbit is circular. By adopting $e = 0.00$ we can therefore solve for the optimal values of the orbital semi-amplitudes K ’s and center-of-mass motion γ , as described in Section 3.1. The orbit velocity curves are shown in Figure 3, and the physical parameters are given in Table 7. The minimum masses are essentially identical for the two components, $17.1 \pm 0.3M_{\odot}$ and $17.2 \pm 0.3M_{\odot}$. The radial velocity curves show good agreement with the data.

As a further check we have plotted the data in a Wilson diagram (Wilson 1941; see Section 3.1) shown in Figure 4. In obtaining the “best fit” it would be inappropriate to use standard linear least-squares fitting (e.g., Bevington 1969) as there are errors associated with both the ordinate and abscissa. Following Section 15.3 of Press et al. (1997)¹⁷, we determine the best “straight line fits” and their associated errors explicitly including our error estimates for both v_1 and v_2 . We compare the orbital results with the Wilson’s results in Table 8. Note the good agreement both in γ and in K_1/K_2 , and recall that for Wilson’s method to work we make no use of the phase information or even the periods.

For the light curve analysis we started with effective temperatures of 36,500 K and

¹⁷See also the excellent description at <http://mathworld.wolfram.com/LeastSquaresFitting.html>.

35,000, somewhat hotter than our spectral types would indicate (Massey et al. 2006) in order to better match the observed absolute magnitude for the system. However, the existent photometry for LMC 172231 is not in good agreement. The out-of-eclipse light-curve magnitude ($V \sim 14.04$) is consistent with Massey (2002)’s $V = 13.96$ and Schild & Testor (1992)’s $V = 14.02$. The *average* reddening of LMC OB stars is $E(B - V) = 0.13$ and so we might expect colors for late O-type dwarfs of $B - V \sim -0.1$ and $U - B \sim -1.0$. Massey (2001) obtains $B - V = +0.10$ and $U - B = -1.14$. These values are inconsistent with each other (the first is too red, and the second too blue), and suggest that the star may have been entering or exiting eclipse when the data were taken. Testor & Niemela (1998) obtained $B - V = -0.08$, close to our expectations, and so for the purposes of computing M_V for the system, we adopt the Testor & Niemela (1998) values¹⁸. Adopting the intrinsic color $(B - V)_0 = -0.26$ of Martins & Plez (2006), we derive $M_V = -5.0 \pm 0.3$ for the system, where the error reflects a modest uncertainty of 0.07 mag in $E(B - V)$, and hence 0.2 mag in A_V , plus another 0.1 mag uncertainty in the distance modulus of the LMC (see van den Bergh 2000).

The preliminary light curve solution yielded an estimate of the flux ratio $F_{V_2}/F_{V_1} \sim 0.9$. We used this with the radial velocity solution to perform a tomographic analysis using seven MagE spectra covering both double-lined quadratures. We fit these with FASTWIND, finding significantly lower effective temperatures than had been first assumed. It was also clear from the model fitting that a flux ratio of 0.8 was more appropriate than 0.9, constrained mostly by the Balmer line depths. A single additional iteration was made fixing the effective temperatures to the values derived from FASTWIND. The flux ratio of 0.8 then yielded the excellent fit to the light curve shown in Figure 1. Note that the light curve model is computed with $e = 0.00$ and shows excellent agreement both the separation of the eclipses *and* the durations of the eclipses, substantiating that the orbit is circular.

The tomographically separated spectra are shown in Figure 2 (*right*). A casual inspection shows that one component is indeed slightly hotter than the other, based upon the relative amounts of He I $\lambda 4471$ and He II $\lambda 4542$. With the tomographically separated spectra, we classify the components as a bit later than we had originally with the blended spectra, and adopt here O9 V and O9.5 V.

The adopted FASTWIND model fits are shown in Figure 5. We have opted to show the fits with the original (non-separated) data as this shows the good agreement not only with the adopted effective temperatures, but also the final flux ratio, and the radial velocity

¹⁸Testor & Niemela (1998)’s $U - B = -0.88$ is redder than expected for its colors, suggesting that the U might be in error.

of the orbit solution. We wound up adopting rotational velocities of 110 km s^{-1} as these gave good fits to the lines, and we note that the synchronous rotation velocities of the two components are $109 \pm 5 \text{ km}^{-1}$ and $101 \pm 5 \text{ km}^{-1}$, in good agreement with these values.

The final masses we derive are $17.5 \pm 0.3 M_{\odot}$ for the O9 V component and 17.6 ± 0.3 for the O9.5 V component. The bolometric luminosities were computed as described above, and are $\log L/L_{\odot} \sim 4.8$ and 4.7 for the O9 V and O9.5 V components, respectively.

It is interesting to note that the orbital *inclination* changed by only 1σ (from $82^{\circ}5 \pm 0.5$ to $83^{\circ}0 \pm 0.5$) by our iterative application of tomography and light-curve analysis. What *did* change significantly were the stellar radii and bolometric luminosities. Since masses are impossible to determine by “inspection” one would expect that the greatest uncertainties in the MLR are the masses. But, this exercise emphasizes that the luminosities of the individual components also require careful analysis. In the end, the total visual luminosity we derive for the system *does* agree with the “observed” values, within the errors. But, the errors are large. Had we instead eschewed the tomographic analysis, and insisted on matching the absolute visual magnitude, we would have adopted effective temperatures and radii that gave just as good a fit to the visual light curve, but would have overestimated the luminosities (we believe) by 0.3 mag. In practice our initial solution had a difference in effective temperatures larger than we adopted, and this led to a different flux ratio as well. The uncertainties in “L” in the MLR may not always have been fully appreciated. We note below (Section 5) that this has implications for using massive eclipsing binaries as distance indicators.

4.2. ST2-28, O7 V + O8 V

The designation ST2-28¹⁹ comes from Schild & Testor (1992), where the star is listed as number 28 in Zone 2, a region that covers the Lucke-Hodge 90 OB association (Lucke & Hodge 1970). The star was also cataloged as [M2002] LMC 163763 by Massey (2002). It was identified automatically as a probable eclipsing binary (MACHO 82.9010.36) in the MACHO database by Alcock et al. (1997)²⁰ with a period of 1.38122 days, half of the 2.762446 day period determined by Derekas et al. (2007) in their reanalysis of the LMC MACHO eclipsing binaries. This period is in good accord with the 2.762456 day period we find from our own data. Our own photometry is summarized in Table 4 and the data given in Table 9. Our light curve is shown in Figure 6. The eclipse depths are nearly identical, as expected from the

¹⁹Known to SIMBAD as [ST92]2-28.

²⁰See VizieR II/247.

similarity in spectral types. The phase difference between primary and secondary eclipses appears to be indistinguishable from 0.5 with both eclipses showing the same duration, further validating our having adopted a circular orbit. It is clear from the spectra that the earlier component is significantly brighter visually.

We show one of the double-lined spectra in Figure 7 *left*. Schild & Testor (1992) classify the star as O8 V. We initially identified double lines by observing the system at quadrature, and classified the components as O7 V and O8 V. Careful subsequent inspection, however, revealed a third component in the He I lines. This component did not change in radial velocity, and it is not obvious in the He II lines. The lack of He II indicates it is a B-type star, a result we confirm below in our tomographic separation of the three components. Presumably it is either a line-of-sight companion, or, more probably, a distant third member of the system.

Our radial velocities were based upon fitting two Gaussians (and indeed the third component is only barely visible at He I), and although the spectral lines of each component appear to be well separated from each other and the stationary third component, we were concerned that the third component could affect our velocities. Therefore we restrict our analysis to the He II lines, as no third component appeared to be present in these lines, except for a faint hint at He II $\lambda 4686$; we confirm this below by our tomographic analysis. The radial velocities are given in Table 10, along with the standard deviation of the means and the number of lines measured.

4.2.1. *Physical Parameters*

Allowing the eccentricity to vary resulted in a best value $e = 0.005 \pm 0.020$, and we therefore adopted a circular orbit. The orbit solution was particularly well determined, and we show the parameters in Table 11 and in Figure 8. The inferred minimum masses $m \sin^3 i$ are 24.6 ± 0.4 for the O7 V primary, and 20.0 ± 0.3 for the O8 V secondary.

Our Wilson plot for this star is shown in Figure 9, and is compared to the orbital parameters in Table 8. The agreement both for the γ velocity and the inverse mass ratio K_1/K_2 is excellent.

Photometry of the star in the literature varies, doubtless due to some observations having been made during eclipse. Massey et al. (2000) found $V = 14.22$ and $B - V = 0.09$, while Massey et al. (2002) found $V = 14.18$, $B - V = 0.06$. These values are considerably brighter than the $V = 14.63$ found by Schild & Testor (1992). Our light-curve suggests $V = 14.15$ outside of eclipse, in accord with the maximum brightness $V = 14.13$ found by

Alcock et al. (1997) in the MACHO data. We adopt $V = 14.15$ and $B - V = 0.09$. The intrinsic color from Martins & Plez (2006) for an O8-O9 V star is $(B - V)_0 = -0.27$, so $M_V = -5.5 \pm 0.3$.

The preliminary light curve solution using effective temperatures of 37,000 and 35,800 K yielded an estimate of the flux ratio $F_{V_2}/F_{V_1} \sim 0.63$, and a contribution of the third component ($F_{V_3}/(F_{V_1} + F_{V_2})$) of about 15% in order to match the observed absolute magnitude, although this is considerably uncertain. Similar to our analysis of LMC 172231 above, we used this with the radial velocity solution to perform a tomographic analysis using a combination of 8 IMACs and 6 MagE spectra covering both double-lined quadratures. Note the model (computed with $e = 0.00$) matches both the eclipse separations and eclipse durations, demonstrating that the orbit is indeed circular.

The tomographically separated spectra are shown in Figure 7 *right*. Comparison to the Sota et al. (2011) atlas suggests that the primary is intermediate between that of O6.5 V and O7 V. Measurement of the equivalent widths (EWs) of He I $\lambda 4471$ and He II $\lambda 4542$ also indicate that the primary is barely on the O7 V dividing line between the two subtypes (Conti & Frost 1977), with $\log W' = \log(\text{EW}(\lambda 4471)/\text{EW}(\lambda 4542)) = -0.09$. We adopt O7 V as the type. The tomographically separated spectrum of the secondary appears to be of O8 V, consistent with our estimation from the blended spectra. The third component contributes so little light to the system that extracting a good spectrum is difficult, and the spectrum is too poor to see either Si IV or Si III; Mg I $\lambda 4481$ is only marginally visible, so we know this is an early B star (B0-2) and not later. There is a hint of He II $\lambda 4686$, which, if real, would suggest a B0 V type.

Our FASTWIND fitting of the tomographically separated primary and secondary components found slightly higher effective temperatures (38,500 and 36,500 K) than what we had initially assumed. For the purposes of finding good values for the flux ratios, we adopted a third component model with an effective temperature of 30,000 K, corresponding to that of a B0 V (Massey et al. 2005). From the depths of the spectral lines we confirmed that the flux ratio F_{V_2}/F_{V_1} must be close to the 0.63 value determined by the light curve, but that the contribution from the tertiary ($F_{V_3}/(F_{V_1} + F_{V_2})$) might be a little higher, probably 0.25²¹. We then performed a second light curve analysis, fixing the effective temperatures and third light-light component. The final flux ratio F_{V_2}/F_{V_1} from this fitting is 0.62 ± 0.02 . The light curve is shown in Figure 6, and the FASTWIND fits to the spectra are shown in Figure 10. The third component is very obvious in the He I lines. The agreement of the

²¹If instead we adopted an effective temperature of 28,000 K for the third component, typical of a B1 V star (Trundle et al. 2007), we obtain similar results.

model fitting to the observed spectra is not perfect, but we judge it adequate. The greatest uncertainty is in the flux contribution of the third component. We have adopted projected rotational velocities of 170 km s^{-1} and 140 km s^{-1} for the primary and secondary, consistent with the synchronous values of $173 \pm 5 \text{ km s}^{-1}$ and $141 \pm 5 \text{ km s}^{-1}$. The lines of the tertiary are sharper, and we adopted 100 km s^{-1} for the fits.

The final masses we derived were $24.9 \pm 0.4 M_{\odot}$ and $20.2 \pm 0.4 M_{\odot}$, with the slightly larger errors due to the larger uncertainty in the orbital inclination i (compared to that of LMC 172231) due to the third light component. The formal error on the inclination for the light curve analysis is $0^{\circ}.5$, but we quote $5^{\circ}.0$, as this is consistent with uncertainty in the third light component. It is worth noting that the radii changed by only 1σ from the original to final fits, despite the changes in the assumed effective temperatures, third light component, and resulting inclination changes. The O7 V and O8 V components have $\log L/L_{\odot} \sim 5.3$ and 5.0 , respectively.

5. The Mass-Luminosity Relationship and Comparison with Stellar Evolutionary Models

In Section 1 we argued that the goal of this project was to provide masses and luminosities that were so well determined that they could serve as *linchpins* in the upper end of the MLR. In addition, we wished to see how well our parameters agreed with the current generation of stellar evolutionary tracks.

In Figure 11 we compare the masses and luminosities of massive stars in young detached eclipsing binary systems, where the data come from Table 1 of Gies (2012) and references therein²². Black points shows the data for the Milky Way stars, while red points shows the data for previously studied LMC stars. Our four LMC stars are shown by green points. The lines denote the expectations from the latest Geneva evolutionary models with solar metallicity ($z = 0.014$ using the Asplund et al. 2009 abundances) shown in black and LMC metallicity ($z = 0.006$) shown in cyan. The solar metallicity tracks are from Ekström et al. (2011) while the LMC metallicity tracks are from Chomienne et al. (2011, in prep)²³. The solid lines correspond to no initial rotation, while the dashed lines correspond to an initial rotation of 40% of the critical velocity.

²²We have updated the effective temperature of SC1-105 to those given by Bonanos et al. (2011).

²³We are indebted to Georges Meynet for forwarding these models and allowing us to use them in advance of publication.

The models emphasize the point we made in Section 1, namely that the mass-luminosity relationship really depends upon age for massive stars. Although the error bars are large for the entire data set, we find it reassuring nearly all of the points are found within the expectations of main-sequence objects. The exceptions are three red (LMC) outliers on the left, which are, in order of decreasing luminosity, the secondary component of SC1-105 (Bonanos 2009; Bonanos et al. 2011) and the primary and secondary components of 78.6097.13 (González et al. 2005).

While this provides good statistical agreement with the evolutionary models, it is not the critical test. In the upper two panels of Figure 12 we show the location of our four components on the H-R diagram with the dynamical masses indicated. (Note that because hotter effective temperatures imply high luminosities, error bars are diagonal lines in this diagram.) Overall the agreement is encouraging. For instance, the components in each system appear to have the same age. We show isochrones at 1 Myr intervals, and the components lie parallel to these dashed lines, indicating that the physical parameters are consistent with the same age for each component, which we would expect. Although the masses are approximately what we expect from their location in the HRD, it is intriguing that the masses for all four components are a bit too low compared to the masses of the tracks. We note that these differences are not due to mass loss. For instance, in the case of LMC 172231, a 5 Myr old star with an initial mass of $20M_{\odot}$ would be expected to have a mass of $19.9M_{\odot}$; i.e., the amount of mass loss expected at these luminosities are small over these time scales.

We can quantify the size of the discrepancy by examining the differences in masses between what we observe and what the models predict by interpolating along an isochrone. We list these differences in Table 12. The “observed” masses come from our orbit solution, and the “Model” mass comes from using our “observed” bolometric luminosities to interpolate along the isochrone using a smooth, high order polynomial fit. Both components of LMC 172231 and ST2-28 have differences in the same sense, that the masses we observe are lower than the masses predicted by the model. Alternately we can ask what bolometric luminosities should correspond to our observed masses. We find (equivalently) that all four components are slightly over-luminous for their mass, by about 0.2 dex. While the discrepancy for the secondary of LMC 172231 is not significant, the others are all significant at the 2-3 σ level. Although these discrepancies are small, it is unsettling that they are all in the same sense. Are there underlying systematic issues that may be in play?

First, we consider our calculated bolometric luminosities. We have adopted the effective temperature determinations from FASTWIND, and if these were systematically too large we would derive too high a bolometric luminosity. But, they would have be off by more

than seems reasonable: to lower the bolometric luminosities by 0.1-0.2 dex would require temperatures that were cooler by about 6-12%, or 2,000-4,000 K. The precision in our fitting the spectra is of order 500 K, and we have formally adopted errors of $\pm 1,000$ K in the propagation of errors in Tables 7 and 11. The agreement between FASTWIND and the “gold standard” hot star model atmosphere CMFGEN (Hillier & Miller 1998) is near perfect in terms of the effective temperatures (Neugent et al. 2010; Massey et al. 2011, in prep). Alternatively, the radii would have to be over estimated by about 12-25%. This, too, seems beyond any reasonable possibility: the radii are fixed by the widths of the eclipse depths and we believe are determined to 3-6 times better than this.

Nevertheless, we have assumed spherical geometry in determining the bolometric luminosities, and used the “volume radius” from the light curve analysis with our FASTWIND effective temperatures. If these stars were so close that tidal distortions were significant, this could be a potential problem, as our effective temperatures really only correspond to those measured at quadrature. Note though that a change of several thousand degrees would correspond to a change 1-2 spectral types during an orbit. Such changes are not seen even in contact systems. In truth, the tidal distortions in our detached systems are very small. Examining the light curves, the lack of significant ellipsoidal variations supports the spherical nature of the objects. In addition GENSYN defines a fill-out factor, the ratio of the photospheric surface to the Roche surface. Any value below unity indicates a detached component, and values below 0.90 correspond to essentially spherical stars. The primary of ST2-28 has the highest fill-out, 0.87, and we can see slight evidence of this in the small ellipsoidal variations in its light curve. However we stress that the distortion of even this star is minimal. As noted above, we have an alternative “tidal model” solution for the bolometric luminosities as well given in Table 7 and 11. The bolometric luminosities implied by these are about 0.06-0.08 dex *larger* than the more conservative values we have been using, which would exacerbate the differences with the evolutionary models.

In the introduction we touted the advantage of studying systems in the Magellanic Clouds rather than in the Milky Way as the distances are known: many methods yield essentially the same answer for the distance of the LMC, and the distance is established to at least 10% (van den Bergh 2000, and references therein). This provides a reality check on whether the luminosities we derive are reasonable or not. In the case of LMC 172231 the observed M_V of the system is -5.0 ± 0.3 mag, while our physical parameters lead to a modeled M_V of -4.6 ± 0.1 mag. The agreement is within the errors, but it suggests that if we had instead adopted effective temperatures that matched the observed M_V our problem would be worse by 0.1-0.2 dex, as matching the observed M_V would lead to a higher luminosity. For ST2-28 the situation is more complex, as the amount of light contributed by the third component adds a complication. The modeled total luminosity of the system

agrees with what we observe when we adopt a third component contamination based upon our spectral fitting, but the uncertainties are large²⁴.

Could the masses themselves be in error? The masses would only have to be low by ~ 10 - 12% . Our reality checks have all agreed: Wilson’s method (which is independent of all phase information) has nearly identical γ -velocities and values for the *ratio* of the orbital semi-amplitudes as that found from our orbit solutions. But what if there were some systematic blending problem that was not being properly accounted for by our measurement technique? We can test this directly by inverting the problem: what would the orbital amplitudes have to be in order to match the masses from the evolutionary models, assuming that the orbital inclination is approximately right. For LMC 172231, matching the evolutionary masses would require that $K_{\text{prim}}=230.1 \text{ km s}^{-1}$ rather than 234.9 km s^{-1} (i.e., 4.8 km s^{-1} smaller), and K_{sec} would have to be 248.8 km s^{-1} , rather than our 233.2 km s^{-1} (i.e., 15.6 km s^{-1} larger). For ST2-28 the differences are even greater: to match the model masses, K_{prim} would have to be 254.0 km s^{-1} rather than 241.0 km s^{-1} (i.e., 13.0 km s^{-1} larger) and K_{sec} would have to be 316.4 km s^{-1} rather than 297.0 km s^{-1} (i.e., 19.4 km s^{-1} larger). In Figure 13 we show how the required values would compare with an observed spectrum *vs* how the measured values compared. The agreement for He I $\lambda 4922$ in LMC 172231 is shown in the upper two panels, with the shifts on the left being computed by what would be required to match the evolutionary masses, while the shifts on the right are based upon our measured orbital amplitudes. The difference is negligible for the primary, but it is clear from the secondary that our adopted velocity is a better fit. The He II $\lambda 4542$ line in ST2-28 is shown in the bottom two panels. Again on the left we show the shifts required to bring the masses into agreement with the evolutionary values, while on the right we show the shifts based upon our adopted velocities. The latter is clearly better.

We were of course curious to see if other systems show similar discrepancies. Comparisons at this level of precision between the binary and evolutionary masses are usually not possible; it requires both very good mass determinations *and* careful effective temperatures determinations for the bolometric luminosities. Two studies that meet these criteria are that of SC1-105²⁵ (by Bonanos 2009) and of the LH54-425 (by Williams et al. 2008), both LMC binaries. We compare their masses to those expected from the evolutionary tracks in the

²⁴We do note that as a cautionary tale to our colleagues attempting to derive distances to nearby galaxies from such binaries that the errors associated are larger than are sometimes estimated, as we see in the comparisons here. For a contrasting view, see Bonanos et al. (2011).

²⁵The star is more commonly known as W28-22 from Westerlund (1961) or LH81-22 from Lucke (1972); see Table 2 in Massey et al. (2000).

lower part of Figure 12²⁶.

Bonanos (2009) describes the components of SC1-105 as highly non-coeval, with ages of 5 Myr (primary) and >10 Myr using the older (non-rotating) Geneva evolutionary tracks, and cites this as evidence that there has been significant mass transfer. We see in Figure 12 that in fact both components neatly fall along a single isochrone (5 Myr) with the newer Geneva tracks that include the effects of rotation, and are in fact quite coeval. The components of SC1-105 are late O-type dwarfs, similar to those studied here. The secondary is highly over-luminous for its mass. We agree that the system is semi-detached, with the secondary filling its Roche lobe. However, her fit of the light-curve significantly fails to match the eclipse depths for both the primary and secondary eclipses by 0.1 mag or more, a problem she attributes to “spots”. Rather, we believe this is indicative of a well-known problem in analyzing contact and semi-detached systems. In such systems the orbital semi-amplitudes are significantly over-estimated using low-excitation optical lines, with smaller K values obtained from the UV (see, for example, Penny et al. 2008) The physical explanation is that the side of the star in overflow that is facing its companion is producing weaker optical lines because the temperature gradient is less steep there. The center of light of the optical lines is thus skewed toward the outer parts of the star, giving a spuriously large K . This overestimates the separation of the two stars, producing more shallow model eclipses than what is actually seen. Unless one corrects for this by using only high-excitation lines one will derive masses that are too large, as well as spurious values for the other physical parameters²⁷. Note that since the 5 Myr isochrone is almost vertical in the HRD, a change in luminosity (due to an incorrect radius) would have little effect on the derived ages as long as the same effective temperatures were adopted.

LH54-425 consists of earlier O-type stars than what we are studying here, but the sense and the size of the mass discrepancy is very similar to what we find here (Figure 12, *lower right*): both components are slightly over-luminous for their masses (or, conversely, under-massive for their luminosities) when compared to the evolutionary tracks. Note we find that the components are highly coeval, according to the isochrones, with an age of 2.0 Myr, slightly larger than the 1.5 Myr derived by Williams et al. (2008). We have added the differences between the observations and the models to the end of Table 12. We can see that the masses for LH54-425 are discrepant with theory in the same sense, and by the same amount, as what we find here. The result is also only marginally significant, however, when

²⁶In making the figure we have updated the effective temperatures to those found by Bonanos et al. 2011.

²⁷We note that despite these problems Bonanos et al. (2011) successfully used this system to derive a realistic value for the distance of the LMC.

compared to the errors.

The mass-loss rates assumed in the evolutionary models are unlikely to be the culprit. The Geneva models rely upon the Vink et al. (2001) mass-loss laws for O stars, and for $20M_{\odot}$ stars (similar to the mass of those discussed here), the mass loss rate averaged over the first 5 Myr are indeed very low, about $0.02 \times 10^{-6}M_{\odot} \text{ yr}^{-1}$. Puls et al. (1996) did not measure mass-loss in the LMC for stars as low luminosity as these, but did find values $< 0.1 \times 10^{-6}M_{\odot} \text{ yr}^{-1}$ for LMC O-type stars that were considerably more luminous. Similarly Massey et al. (2004, 2005, 2009) find mass-loss rates for LMC O stars with $\log L/L_{\odot}$ of 5.0 to be $< 0.1 \times 10^{-6} \text{ yr}^{-1}$. In order to account for the discrepancy we find, the mass-loss rates would have to be about $0.2\text{-}0.5 \times 10^{-6}M_{\odot} \text{ yr}^{-1}$ for LMC 172231, and $0.9 - 1.0 \times 10^{-6}M_{\odot} \text{ yr}^{-1}$ for ST2-28. These high rates can be ruled out observationally for radiatively-driven winds.

What if instead binary evolution (i.e., Roche-lobe induced mass-loss) has raised the mass-loss rates? We see no evidence of this at present. Certainly in the case of LMC 172231 and ST2-28 we see little current evidence: as discussed above, the stars are not significantly distorted. The residual nebular contamination at $H\alpha$ in the tomographically separated spectra precludes our making an estimate of the mass-loss rate directly.

Is this a problem restricted to that of the LMC? Unfortunately none of the massive young detached Galactic systems listed by Gies (2012) have undergone a similar sort of analysis; at best, the effective temperatures have come from assigning spectral types, usually without tomographic separation. The *masses* of these systems are likely well determined, but their bolometric *luminosities* are not. (This can be inferred from an inspection of the error bars in Figure 11.)

One intriguing possibility has to do with the metallicity we have assumed for the LMC, using a $z = 0.006$ for the LMC based upon the Asplund et al. (2009) abundances. What if the appropriate abundance was a little bit higher or a little bit lower? Would that be enough to explain our discrepancy? To investigate the effect of abundances on the derived masses from the models, we used the solar metallicity ($z = 0.014$) Geneva models for comparison, re-deriving the ages and constructing new isochrones. In all cases the evolutionary masses are about 7% higher for a given luminosity. (At a given age the mass for a particular luminosity is actually *lower* for Galactic metallicity than for the LMC, but the isochrones are shifted to cooler temperatures and so one derives a younger age for these stars, and that results in a higher expected mass.) The median change needed in the models (Table 12) is about 11%. There is no reason to believe this effect is linear, but if it were, explaining the discrepancy by metallicity would require the appropriate models to have much lower metallicities ($z = 0.002$), lower than what is allowed by observations. Of course, given the complicated nature (isochrones shifting and different luminosity for a given mass), it might

be that even slightly lower (or even slightly higher) metallicity models might help alleviate the problem. As more models become available, it will be interesting to test this.

We note that the discrepancy between the dynamical masses and the evolutionary masses we find here is in the same sense as that of the mass discrepancy discussed in the introduction, namely that the masses inferred from the evolutionary tracks are larger masses than those inferred from the surface gravities derived from fitting model atmospheres. But, there the size of the discrepancy is much larger, sometimes a factor of 2 or more, when present. We cannot, however, use our FASTWIND modeling to obtain a useful additional estimate of the mass. The uncertainty in fitting $\log g$ to the tomographically separated spectra is about 0.2 dex. An error of 0.2 dex translates to an uncertainty of 60% in the masses, making this not useful for weighing in on the sort of 15% differences we are seeing here. In addition, we note that FASTWIND produces values for $\log g$ that are systematically about 0.05-0.10 dex smaller than those found using CMFGEN (Neugent et al. 2010; Massey et al. 2011, in prep.). We note that our FASTWIND modeling found a $\log g$ of 4.0 dex [cgs], which is consistent with the $\log g$ values we list in Tables 7 and 11, derived from the masses and radii from our analysis.

We believe this emphasizes the need for such fundamental data such as ours. With queue or robotic observing on small imaging telescopes, and modern spectrographs on large apertures, obtaining excellent photometry and radial velocities and hence very accurate masses is now standard. However, simply relying upon spectral types to assign effective temperatures do not result in bolometric luminosity determinations that are accurate enough to contribute to the discussion.

If the trend is real, what then could be the problem with the models? Either a higher initial rotation than assumed, or convective overshooting, would extend the size of the convective core in the model, resulting in higher luminosity at a given mass. Ribas et al. (2000) have argued that convective overshooting is more significant at higher masses, and this may be consistent with what we observe here. (We are indebted both to the anonymous referee and to Georges Meynet for correspondence on this point.)

Although our empirical data do show a slight “mass discrepancy” between the Keplerian masses, perhaps the real emphasis should be on how well the observations do in fact confirm the evolutionary masses. This is perhaps the most stringent comparison made for high mass stars, and we should be encouraged that the agreement is as good as it is in the masses. It is also encouraging that observation and analysis tools have advanced to the point where one can worry about a discrepancy of order 10% in the masses of these stars. Analysis in future papers will either confirm or refute this as a real trend.

We are grateful to the various observers who were involved in taking imaging as part of our photometric monitoring, and to the SMARTS queue managers Jenica Nelan and Michelle Buxton. It was also a pleasure to work with Suzanne Tourtellotte, the SMARTS data manager, who kept the data pipeline flowing, helped us retrieve missing images whenever we made mistakes, and provided some of the most challenging password clues we've ever encountered. A number of undergraduate students were involved in the early stages of examining the photometry data, including Erin Darnell, Corey Ritter, Shaye Storm, and Yelena Tsitkin. Darnell also performed a preliminary reduction of the early Swope data. Brian Skiff looked after the data transfer of the images from Yale daily for several observing seasons, and offered good advice. Vincent Chomienne and Georges Meynet generously made the Geneva models available for our use. Larry Wasserman was kind enough to run our velocity data through his orbit program in order to ascertain whether or not the velocity data were consistent with a circular orbit. Alceste Bonanos, Georges Meynet, Noel Richardson, and Stephen Williams all offered comments on an early draft of the manuscript. We thank an anonymous referee for helping us improve the paper. This work was supported by the National Science Foundation under awards AST 0506541, 0506573, 0506577, 0506749, 0946314, and 1008020. We are grateful for the excellent support we received at Las Campanas during the course of this project; it is always a pleasure and privilege to observe on that mountaintop. We also gratefully acknowledge the patience and encouragement of the Carnegie and Arizona TACs who were generous with time allocation on the two Magellan telescopes.

Facilities: Magellan:Baade, Magellan:Clay, :Swope, CTIO:1.0m, CTIO:1.3m

REFERENCES

- Alcock et al. 1996, ApJ, 470, 583
- Alcock et al. 1997, AJ, 114, 326
- Asplund, M., Grevesse, N., Sauval, A. J., & Scott, P. 2009, ARA&A, 47, 481
- Bagnuolo, W. G., & Gies, D. R. 1991, ApJ, 376, 266
- Bagnuolo, W. G., & Gies, D. R. 1992, in *Complementary Approaches to Double and Multiple Star Research*, ASP Conf. Ser. 32, ed. H. A. McAlister and W. I. Hartkopf (San Francisco: ASP), 140
- Batten, A. H. 1973, *Binary and Multiple Systems of Stars*, (Oxford: Pergamon Press), 17
- Bevington, P. 1969, *Data Reduction and Error Analysis for the Physical Sciences* (NY: McGraw-Hill), 110
- Binnendijk, L. 1960, *Properties of Double Stars* (Oxford: Oxford University Press), 69
- Bohannon, B., & Conti, P. S. 1976, ApJ, 204, 797
- Bonanos, A. Z. 2009, ApJ, 691, 407
- Bonanos, A. Z., et al. 2006, ApJ, 652, 313
- Bonanos, A. Z., Castro, N., Macri, L. M., & Kudritzki, R.-P. 2011, ApJ, 739, 9
- Breysacher, J. 1981, A&AS, 43, 203
- Breysacher, J., Azzopardi, M., & Testor, G. 1999, A&AS, 137, 117
- Burkholder, V., Massey, P., Morrell, N. 1997, ApJ, 490, 328
- Claret, A. 2000, A&A, 3636, 1081
- Coluzzi, R. 1993, BICDS, 43, 7
- Conti, P. S., Ebbets, D., Massey, P., & Niemela, V. S. 1980, ApJ, 238, 184
- Conti, P. S., & Frost, S. A. 1977, ApJ, 212, 728
- Conti, P. S., Leep, E. M., & Lorre, J. J. 1977, ApJ, 214, 759
- Conti, P. S. & Walborn, N. R. 1976, ApJ, 207, 502
- Derekas, A., Kiss, L. L., & Bedding, T. R. 2007, ApJ, 663, 249
- Eddington, A. S. 1924, MNRAS, 84, 208
- Ekström, S. et al. 2011, A&A, submitted
- Evans, C. J., Lennon, D. J., Smartt, S. J., & Trundle, C. 2006, A&A, 456, 623

- Faccioli, L., Alcock, C., Cook, K., Prochter, G. E., Protopapas, P., & Pyphers, D. 2007, *AJ*, 134, 1963
- Fitzpatrick, E. L., et al. 2003, *ApJ*, 587, 685
- Gies, D. R. 2003, in *A Massive Star Odyssey, from Main Sequence to Supernova, IAU 212*, ed. K. A. van der Hucht, A. Herrero, & C. Esteban (San Francisco: ASP), 91
- Gies, D. R. 2004, in *Spectroscopically and Spatially Resolving the Components of the Close Binary Stars*, ASP Conf. Ser. 318 (San Francisco: ASP), 61
- Gies, D. R. 2012, in *Four Decades of Research on Massive Stars: A Scientific Meeting in Honour of Anthony F. J. Moffat*, (ASP Conf. Ser. vol.), ed. C. Robert, N. St-Louis, & L. Drissen (San Francisco: ASP), in press
- González, J. F., Ostrov, P., Morrell, N., & Minniti, D. 2005, *ApJ*, 624, 946
- Guinan, E. F., et al. 1998, *ApJ*, 509, L21
- Hamuy, M. et al. 2006, *PASP*, 118, 2
- Harries, T. J., Hilditch, R. W., & Howarth, I. D. 2003, *MNRAS*, 339, 157
- Henry, T. J., Franz, O. G., Wasserman, L. H., Benedict, G. F., Shelus, P. J., Ianna, P. A., Kirkpatrick, J. D., & McCarthy, Jr., D. W. 1999, *ApJ* 512, 864
- Herrero, A., Kudritzki, R. P., Vilchez, J. M., Butler, K., & Haser, S. 1992, *A&A*, 261, 209
- Hilditch, R. W., Howarth, I. d., Harries, T. J. 2005, *MNRAS*, 357, 304
- Hillier, D. J., & Miller, D. 1998, *ApJ*, 496, 407
- Hubeny, I., & Lanz, T. 1995, *ApJ*, 439, 875
- Hutchings, J. B. 1968a, *MNRAS*, 141, 219
- Hutchings, J. B. 1968b, *MNRAS*, 141, 329
- Hutchings, J. B. 1969, *MNRAS*, 144, 235
- Hutchings, J. B. 1970a, *MNRAS*, 147, 161
- Hutchings, J. B. 1970b, *MNRAS*, 147, 367
- Hutchings, J. B. 1979, in *Mass Loss and Evolution of O-type Stars*, IAU Symp. 83, ed. P. S. Conti & C. W. H. de Loore (Dordrecht: Reidel), 3
- Hunter, I., Lennon, D. J., Dufton, P. L., Trundle, C., Simon-Diaz, S., Smartt, S. J., Ryans, R. S. I., & Evans, C. J. 2008, *A&A*, 479, 541
- Lafleur, J., & Kinman, T. D. 1965, *ApJS*, 11, 216
- López-Morales, & Clemens, J. C. 2004, *PASP*, 116, 22

- Lucke, P. B. 1972, PhD Thesis, Univ. Washington
- Lucke, P. B., & Hodge, P. W. 1970, *AJ*, 75, 171
- Mace, G. N., Prato, L., Wasserman, L. H., Schaefer, G. H., Franz, O. G., & Simon, M. 2009, *AJ*, 137, 3487
- Maeder, A., & Meynet, G. 2000, *ARA&A*, 38, 143
- Martins, F., & Plez, B. 2006, *A&A*, 457, 637
- Massey, P. 2002, *ApJS*, 141, 81
- Massey, P., Bresolin, F., Kudritzki, R.-P., Puls, J., & Pauldrach, A. W. A. 2004, *ApJ*, 608, 1001
- Massey, P., & Conti, P. S. 1977, *ApJ*, 218, 431
- Massey, P., & Hanson, M. M. 2012, in *Planets, Stars and Stellar Systems, Vol 2: Astronomical Techniques and Standards*, ed. H. Bond (New York: Springer), in press; arXiv:1010.5270
- Massey, P., & Hunter, D. A. 1998, *ApJ*, 493, 180
- Massey, P., Olsen, K. A. G., Hodge, P. W., Jacoby, G. H.; McNeill, R. T., Smith, R. C., Strong, Shay B. 2007, *AJ*, 133, 2393
- Massey, P., Olsen, K. A. G., Hodge, P. W., Strong, S. B.; Jacoby, G. H.; Schlingman, W.; Smith, R. C. 2006, *AJ*, 131, 2478
- Massey, P., Parker, J. W., & Garmany, C. D. 1989, *AJ*, 98, 1305
- Massey, P., Penny, L. R., & Vukovich, J. 2002, *ApJ*, 565, 982
- Massey, P., Puls, J., Pauldrach, A. W. A., Bresolin, F., Kudritzki, R. P., & Simon, T. 2005, *ApJ*, 627, 477
- Massey, P., Waterhouse, E., DeGioia-Eastwood, K. 2000, *AJ*, 119, 2214
- Massey, P., Zangari, A. M., Morrell, N. I., Puls, J., DeGioia-Eastwood, K., Bresolin, F., & Kudritzki, R.-P. 2009, *ApJ*, 692, 618
- Melnick, J. 1985, *A&A*, 153, 235
- Meynet, G., & Maeder, A. 2000, *A&A*, 361, 101
- Mochnecki, S. W., & Doughty, N. A. 1972, *MNRAS*, 156, 51
- Moore, C. E. 1972, *A Multiplet Table of Astrophysical Interest, Revised Edition* (Boulder: National Bureau of Standards)

- Morrell, N. I., Gonzalez, J. F., Ostrov, P. G., & Minniti, D. 2007, in *Massive Stars in Interacting Binaries*, ASP Conf. 367, ed. N. St-Louis & A. F. J. Moffat (San Francisco: ASP), 77
- Morrell, N. I., Ostrov, P., Massey, P., & Gamen, R. 2003, *MNRAS*, 341, 583
- Morrison, N. D., & Conti, P. S. 1978, *ApJ*, 224, 558
- Morrison, N. D., & Conti, P. S. 1980, *ApJ*, 239, 212
- Neugent, K., Massey, P., & Hillier, D. J. 2010, *BAAS*, 42, 344
- Niemela, V. S., & Morrell, N. I. 1986, *ApJ*, 310, 715
- Niemela, V. S., Morrell, N. I., Fernández Lajús, E., Barbá, R., Albacete Colombo, J. F., & Orellana, M. 2006, *MNRAS*, 367, 1450
- North, P., Gauderon, R., Barblan, F., & Royer, F. 2010, *A&A*, 520, A74
- ed. F. Bresolin, P. A. Crowther, & J. Puls (Cambridge: Cambridge University Press), 71
- Paczynski, B 1997, in *The Extragalactic Distance Scale*, ed. M. Livio, M., Donahue, & N. Panagia (Cambridge: Cambridge University Press), 273
- Parker, J. W. 1993, *AJ*, 106, 560
- Penny, L. R., Gies, D. R., Wise, J. H., Stickland, D. J., & Lloyd, C. 2002, *ApJ*, 565, 1050
- Penny, L. R., Ouzts, C., & Gies, D. R. 2008, *ApJ*, 681, 554
- Petrie, R. M. 1962, *Publ. Dom. Astrophys. Obs.*, 12, 111
- Prato, L. 2007, *ApJ*, 657, 338
- Press, W. H., Teukolsky, S. A., Vetterling, W. T., & Flannery, B. P. 1997, *Numerical Recipes in Fortran 77*, (Cambridge: Cambridge Univ Press), 660
- Puls, J. et al. 1996, *A&A*, 305, 171
- Puls, J., Urbaneja, M. A., Venero, R., Repolust, T, Springmann, U., Jokuthy, A., & Mokiem, M. R. 2005, *A&A* 435, 669
- Rauw, G., Crowther, P. A., Eenens, P. R. J., Manfroid, J., & Vreux, J.-M. 2002, *A&A*, 392, 563
- Rauw, G., Sana, H., Antokhin, I. I., Morrell, N. I., Niemela, V. S., Albacete Colombo, J. F., Gosset, E., & Vreux, J.-M. 2001, *MNRAS*, 326, 1149
- Ribas, I., Jordi, C., & Giménez, Á. 2000, *MNRAS*, 318, L55
- Ribas, I., et al. 2005, *ApJ*, 635, L37
- Rosero, V., Prato, L., Wasserman, L. H., & Rodgers, B. 2011, *AJ*, 141, 13

- Sanduleak, N. 1970, *Contrib. Cerro Tololo Inter-American Obs.*, No. 89
- Schaefer, G. H., Simon, M., Prato, L., & Barman, T. 2008, *AJ*, 135, 1659
- Schild, H., & Testor, G. 1992, *A&AS*, 92, 729
- Schwarzenberg-Czerny, A. 1989, *MNRAS*, 241, 153
- Sota, A., et al. 2011, *ApJS*, 193: 24
- Stickland, D. J., Lloyd, C., & Penny, L. R. 1997, *Obs*, 117, 213
- Testor, G., & Niemela, V. 1998, *A&AS*, 130, 527
- Trundle, C., Dufton, P. L., Hunter, I., Evans, C. J., Lennon, D. J., Smartt, S. J., & Ryans, R. S. I. 2007, *A&A*, 471, 625
- Udalski, A., Soszynski, M., Kubiak, M., Petrzynski, G., Wozniak, P., & Zebrun, K. 1998, *AcA*, 48, 563
- van den Bergh, S. 2000, *The Galaxies of the Local Group*, (Cambridge: Cambridge Univ. Press)
- Vink, J. S., de Koter, A., & Lamers, H. J. G. L. M. 2001, *A&A*, 369, 574
- Vilardell, F., Ribas, I., Jordi, C., Fitzpatrick, E. L., & Guinan, E. F. 2010, *A&A*, 509, A70
- Williams, S. J. et al. 2008, *ApJ*, 682, 492
- Wilson, O. C. 1941, *ApJ*, 93, 29
- Westerlund, B. 1961, *Uppsala Astron. Obs. Ann.*, 5, 1
- Wyrzykowski, L., et al. 2004 *Acta Astron.* 54, 1

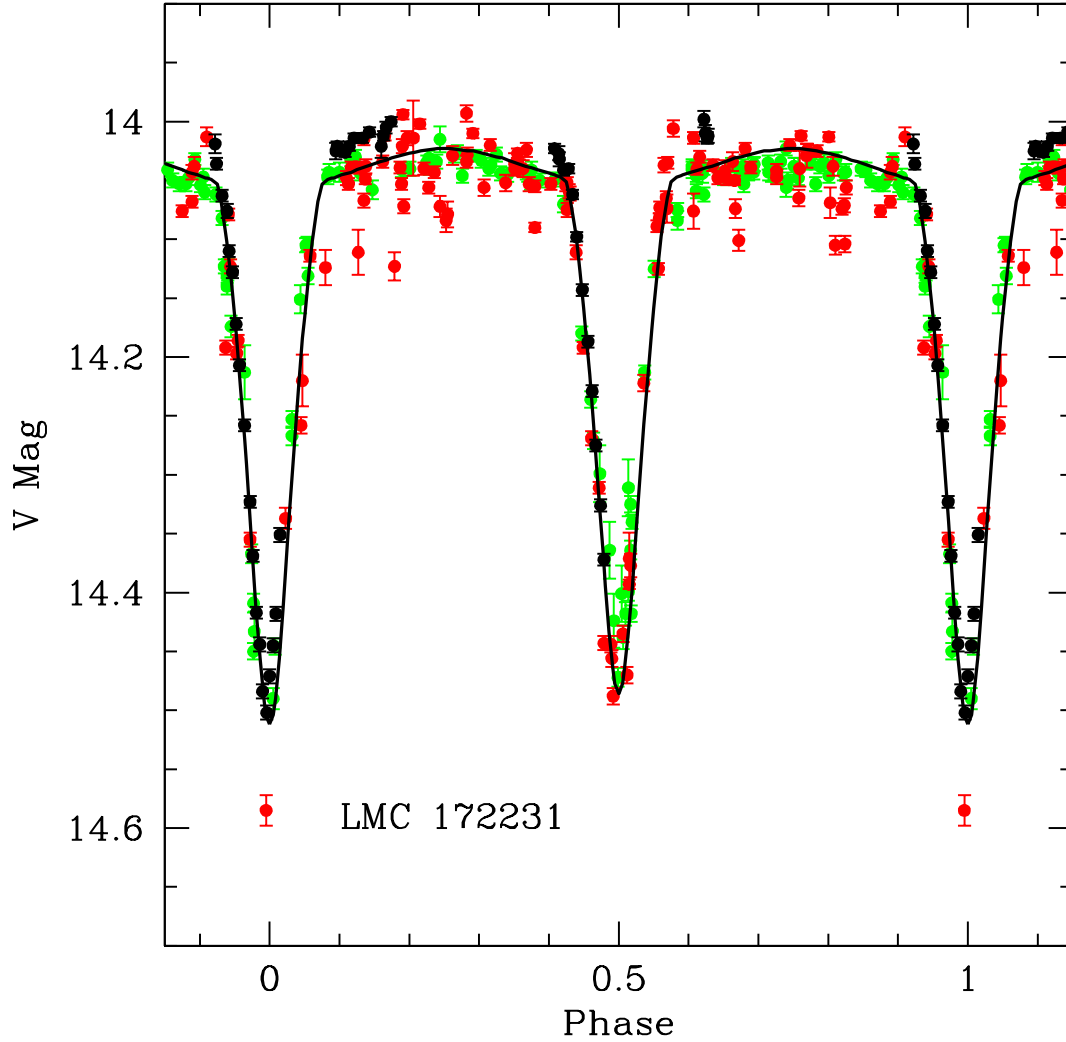


Fig. 1.— Light curve of LMC 172231. The data have been phased using a period of 3.225414 days and a time of primary eclipse of HJD 2453591.469. Black points denote data taken with the Swope 1.0-m telescope, red points denote data taken with the SMARTS Yale 1.0-m telescope, and green points denote data taken with the SMARTS 1.3-m telescope. The light curve model is shown in black.

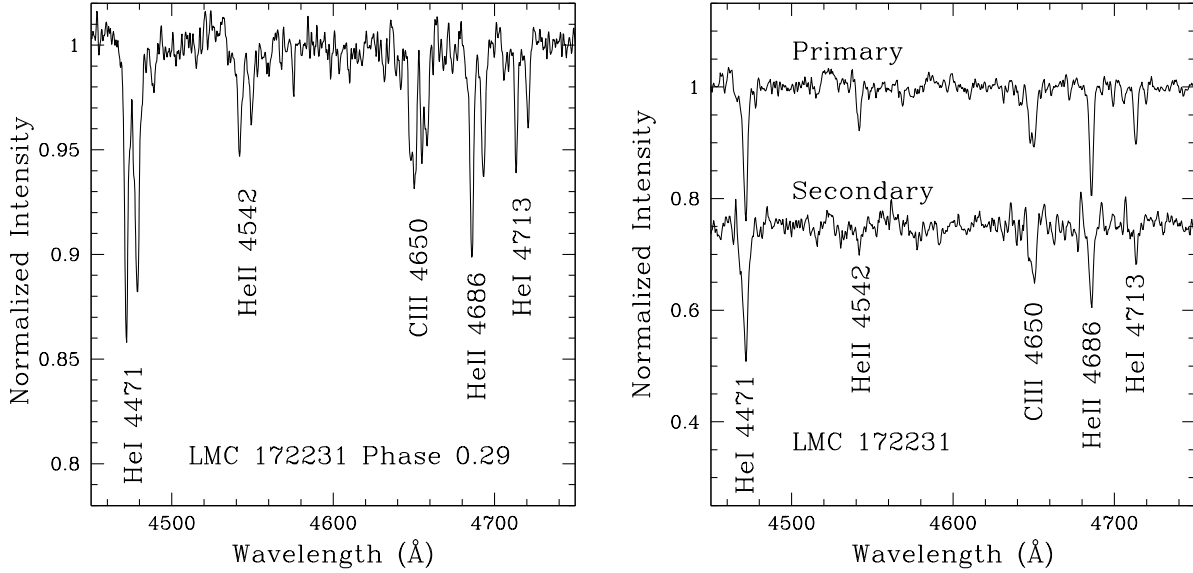


Fig. 2.— Spectrum of the LMC 172231 system. A section of the spectral region of primary importance for classification is shown. *Left:* The data were taken with MagE on HJD 2455143.825, at a phase of 0.29, i.e., just a little over a quarter of a cycle after primary eclipse. The brighter and slightly earlier-type star is blue shifted, while the fainter and slightly later type star is red shifted. The double lines are well separated, except for the CIII blend at $\lambda 4647 - 50 - 51$ which has a complex structure and was not used for radial velocities. The original spectrum has a S/N of 400 per 4-pixel spectral resolution element, and has been smoothed here by a 3-point boxcar average for display purposes. *Right:* The spectra of the individual components separated by tomography. The normalized spectrum of the secondary has been shifted downwards by 0.25 normalized units.

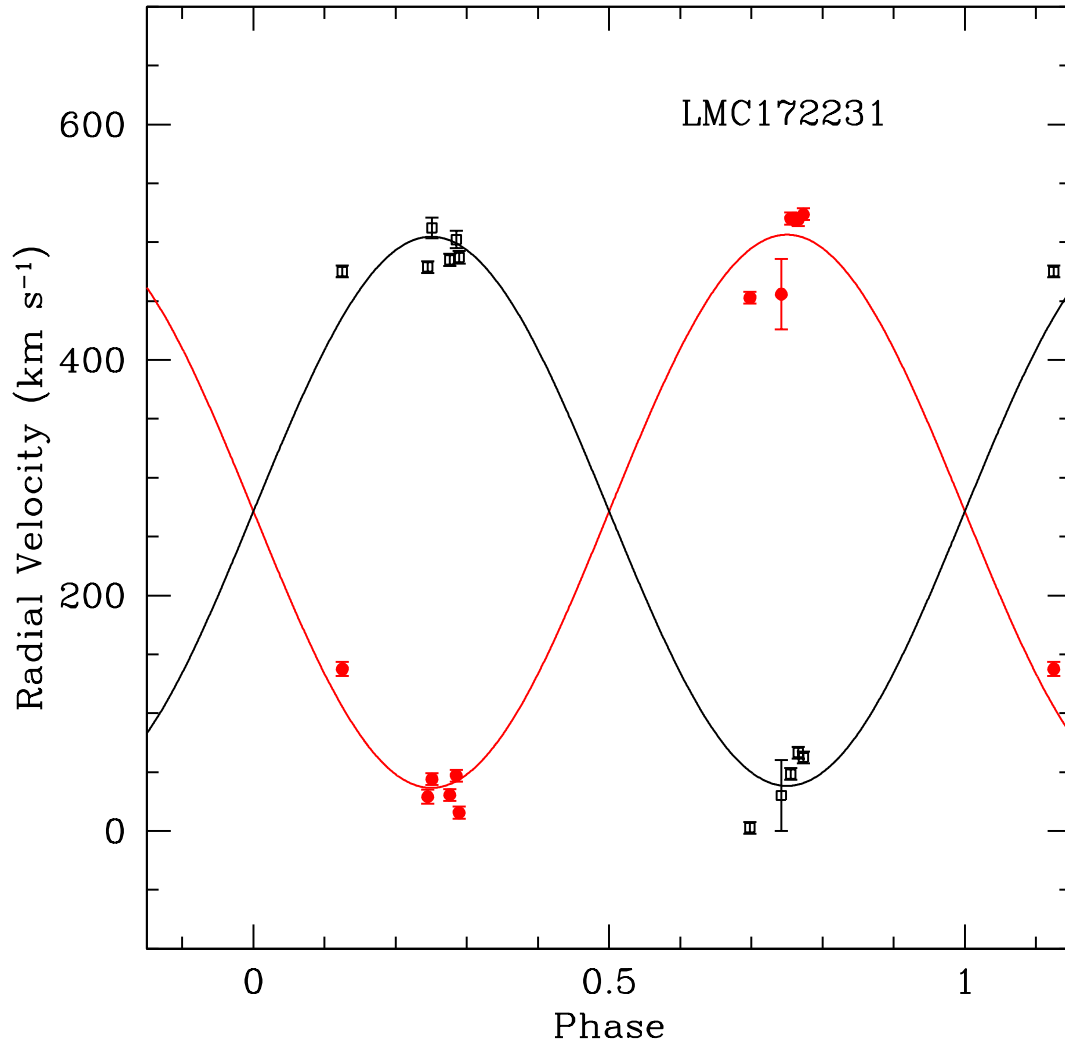


Fig. 3.— Velocity curve for LMC 172231. The radial velocities of the primary (O9 V component) are shown by filled red circles, and the radial velocities of the secondary (O9.5 V component) are shown by black open squares. The red and black curves come from the best fit orbit solutions for the primary and secondary, respectively.

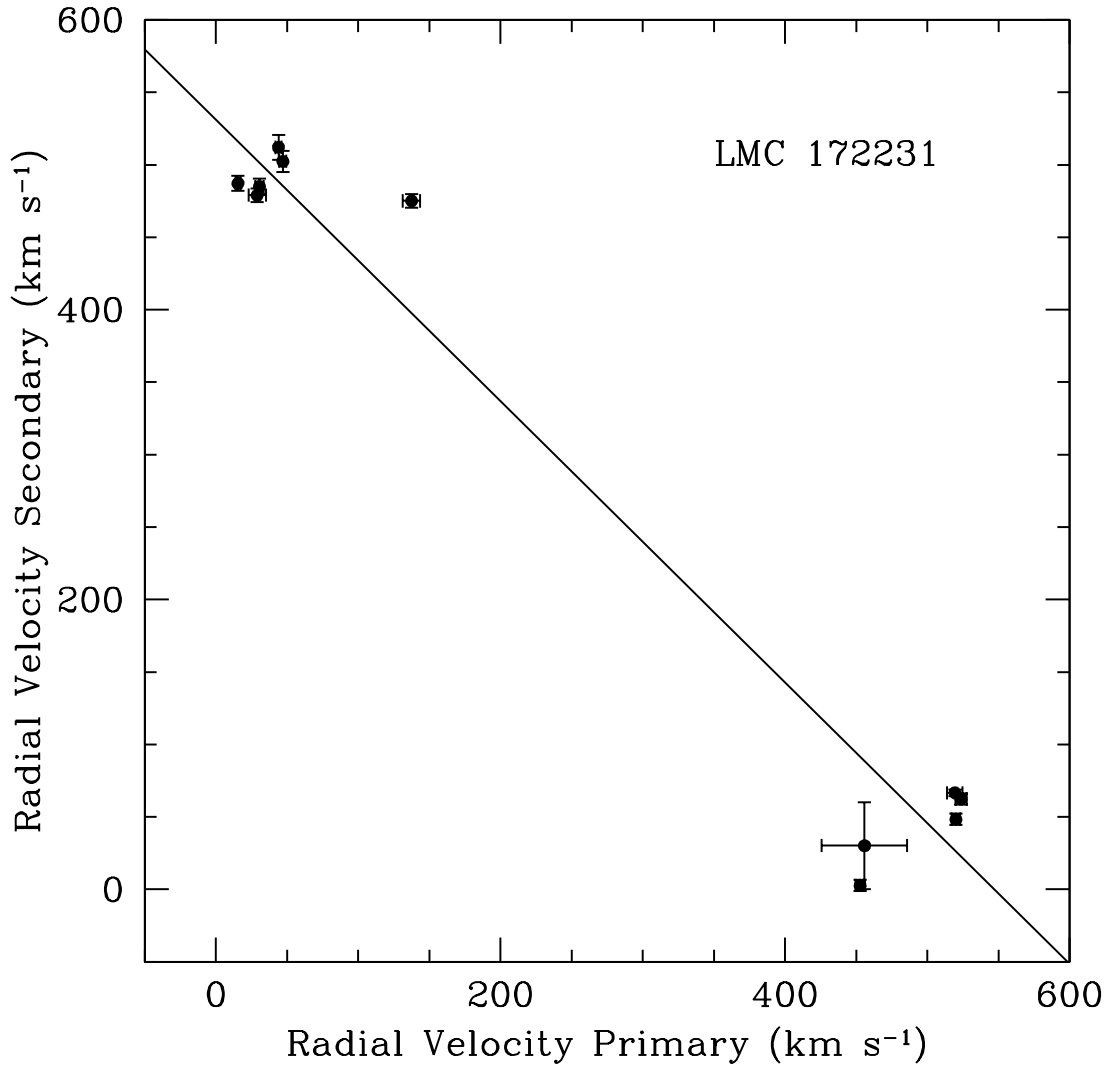


Fig. 4.— Wilson diagram for LMC 172231. The velocities of the two components are shown plotted against each other, along with the best line fit. The slope and intercept are consistent with those derived from the orbit solution shown in Figure 3.

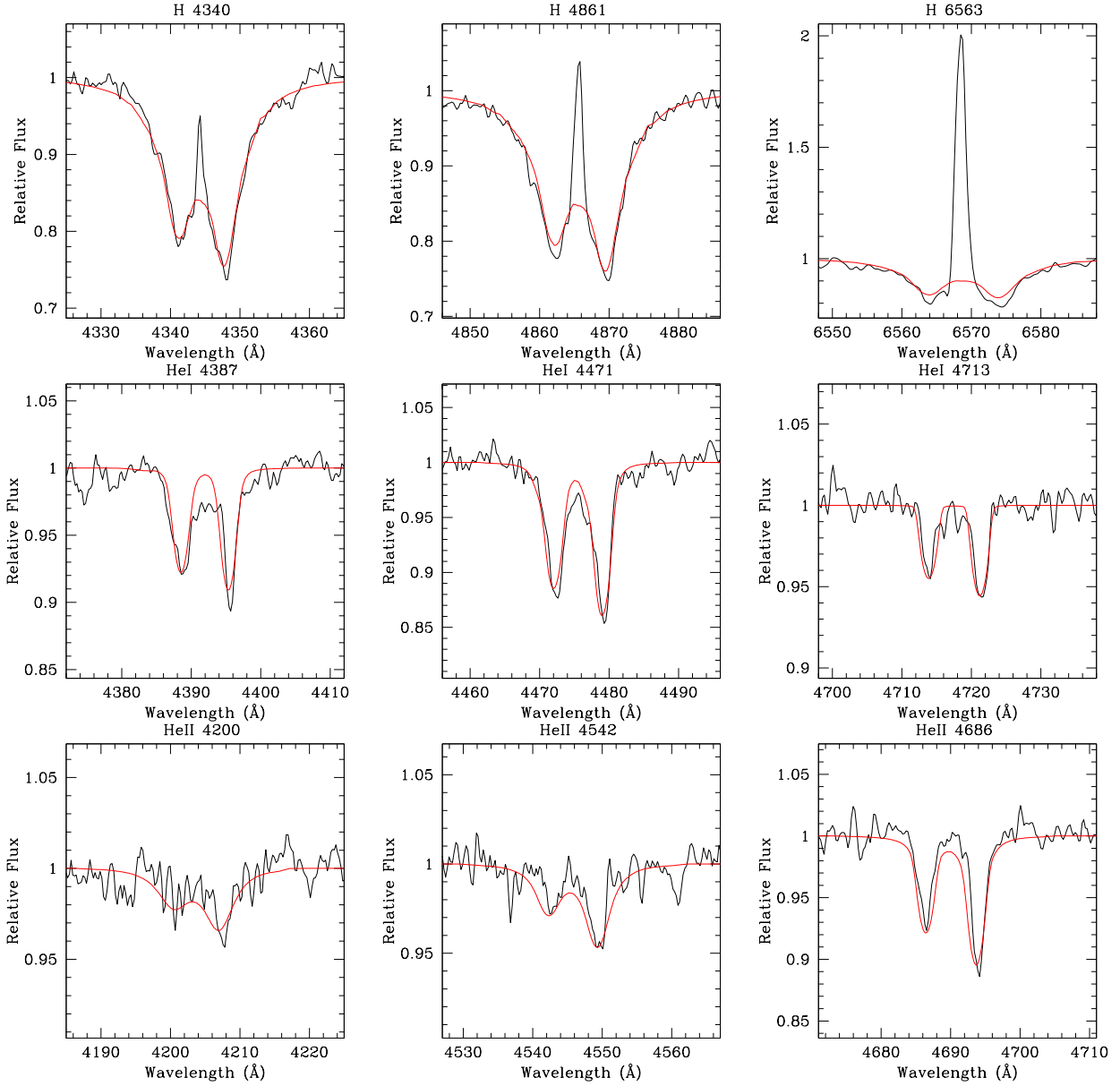


Fig. 5.— LMC 172231 Comparison with Stellar Atmosphere Model. We compare the FAST-WIND models (smooth, red curves) with the observed spectrum. The spectrum used was taken with MagE on HJD 2454877.619 and corresponds to a phase of 0.755. The top row shows the $H\gamma$, $H\beta$, and $H\alpha$ lines; note the presence of some remaining nebular emission at line center. The second row shows the He I $\lambda 4387$, He I $\lambda 4471$, and He I $\lambda 4713$ lines. The bottom row shows the He II $\lambda 4200$, He II $\lambda 4542$, and He II $\lambda 4686$ lines. The latter is primarily sensitive to the mass-loss rate and wind law.

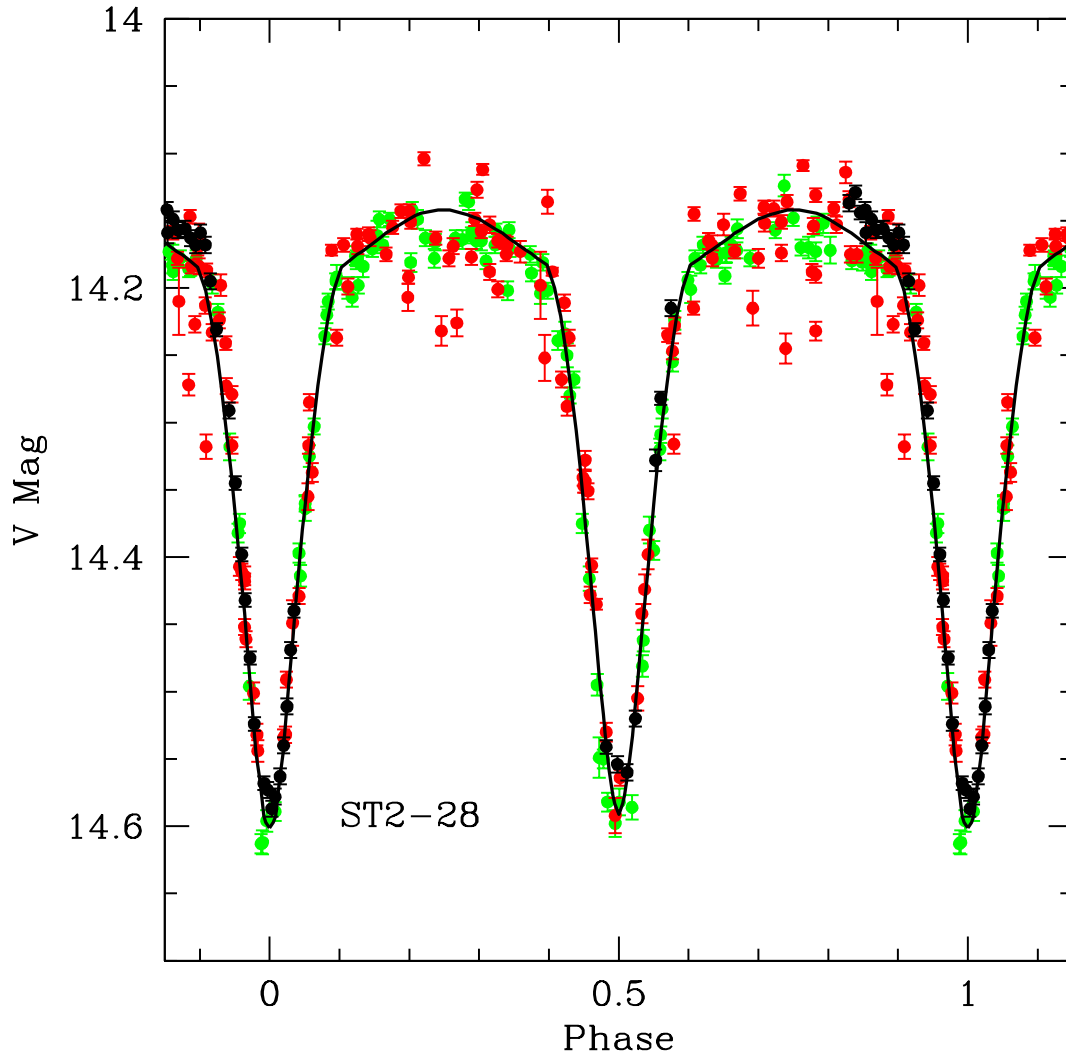


Fig. 6.— Light curve of ST2-28. The data have been phased using a period of 2.762456 days and a time of primary eclipse of HJD 2453590.217. Black points denote data taken with the Swope 1.0-m telescope, red points denote data taken with the SMARTS Yale 1.0-m telescope, and green points denote data taken with the SMARTS 1.3-m telescope. The light curve model is shown in black.

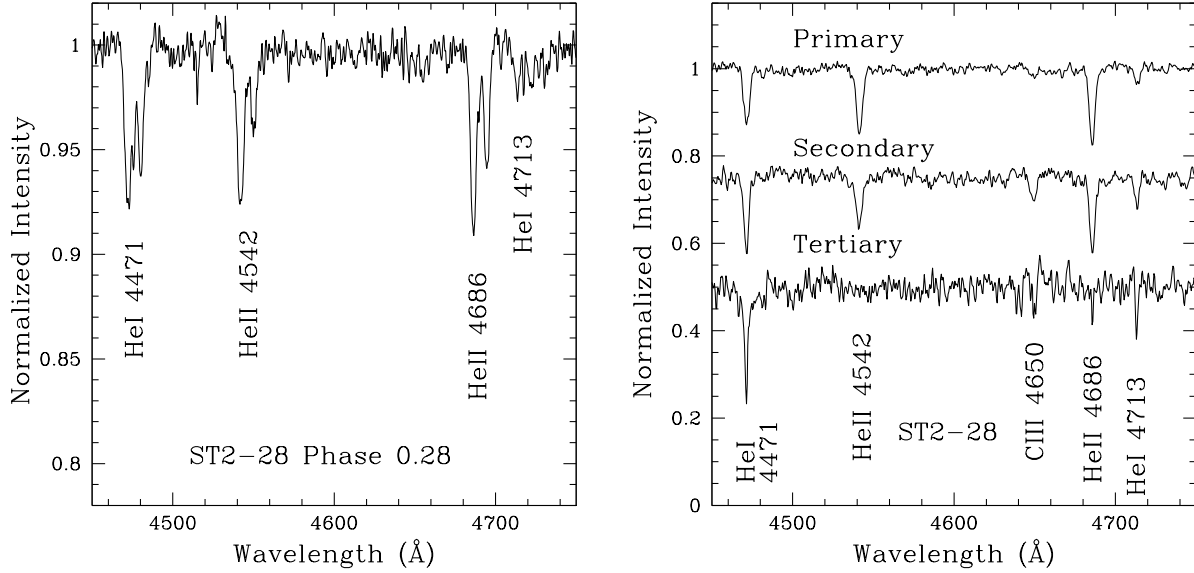


Fig. 7.— Spectrum of the ST2-28 system. A section of the spectral region of primary importance for classification is shown. *Left:* The data were taken with MagE on HJD 2455140.732 at a phase of 0.28, i.e., just a little over a quarter of a cycle after primary eclipse. The brighter and slightly earlier-type star is blue shifted, while the fainter and slightly later type star is red shifted. The double lines are well separated. The third component is barely visible as a small blip in the He I $\lambda 4471$ line. Only the He II lines were used for the orbit solution. The original spectrum has a S/N of 330 per 4-pixel spectral resolution element, and has been smoothed here by a 3-point boxcar average for display purposes. *Right:* The spectra of the individual components separated by tomography. The normalized spectrum of the secondary has been shifted downwards by 0.25 normalized units, and that of the tertiary has been shifted downwards by 0.5 normalized units.

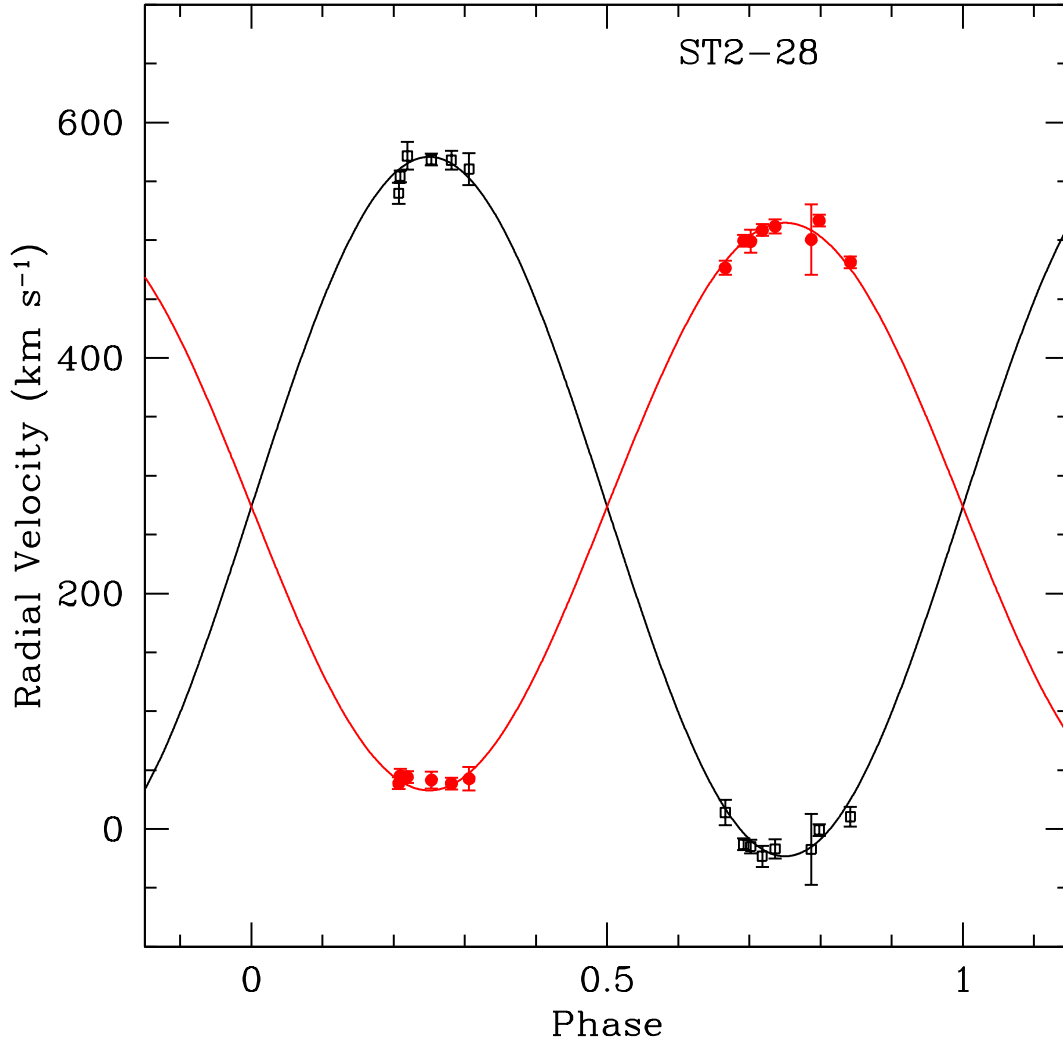


Fig. 8.— Velocity curve ST2-28. The radial velocities of the primary (O7 V component) are shown by filled red circles, and the radial velocities of the secondary (O8 V component) are shown by black open squares. The red and black curves come for the best fit orbit solutions for the primary and secondary, respectively.

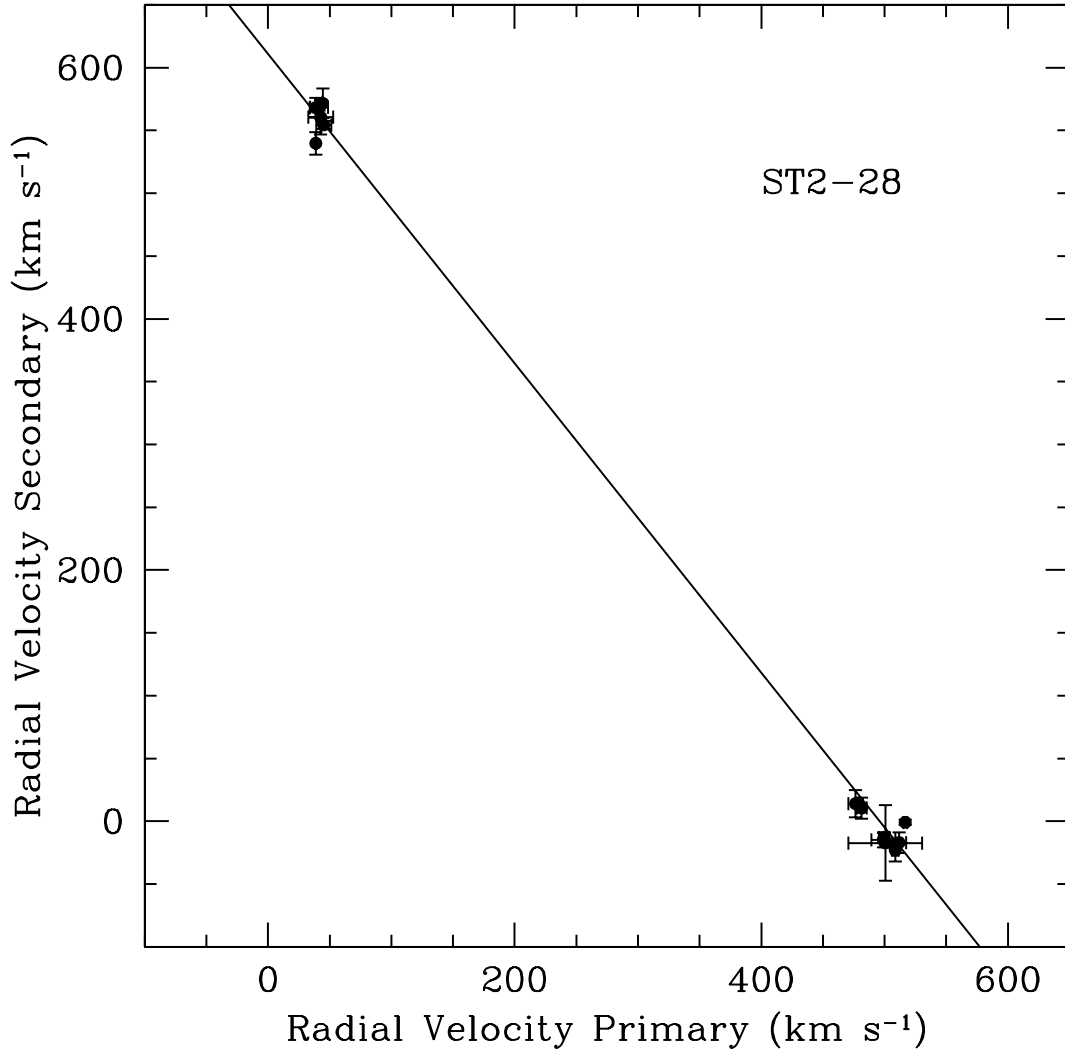


Fig. 9.— Wilson Diagram ST2-28. The velocities of the two components are shown plotted against each other, along with the best line fit. The slope and intercept are consistent with those derived from the orbit solution shown in Figure 8.

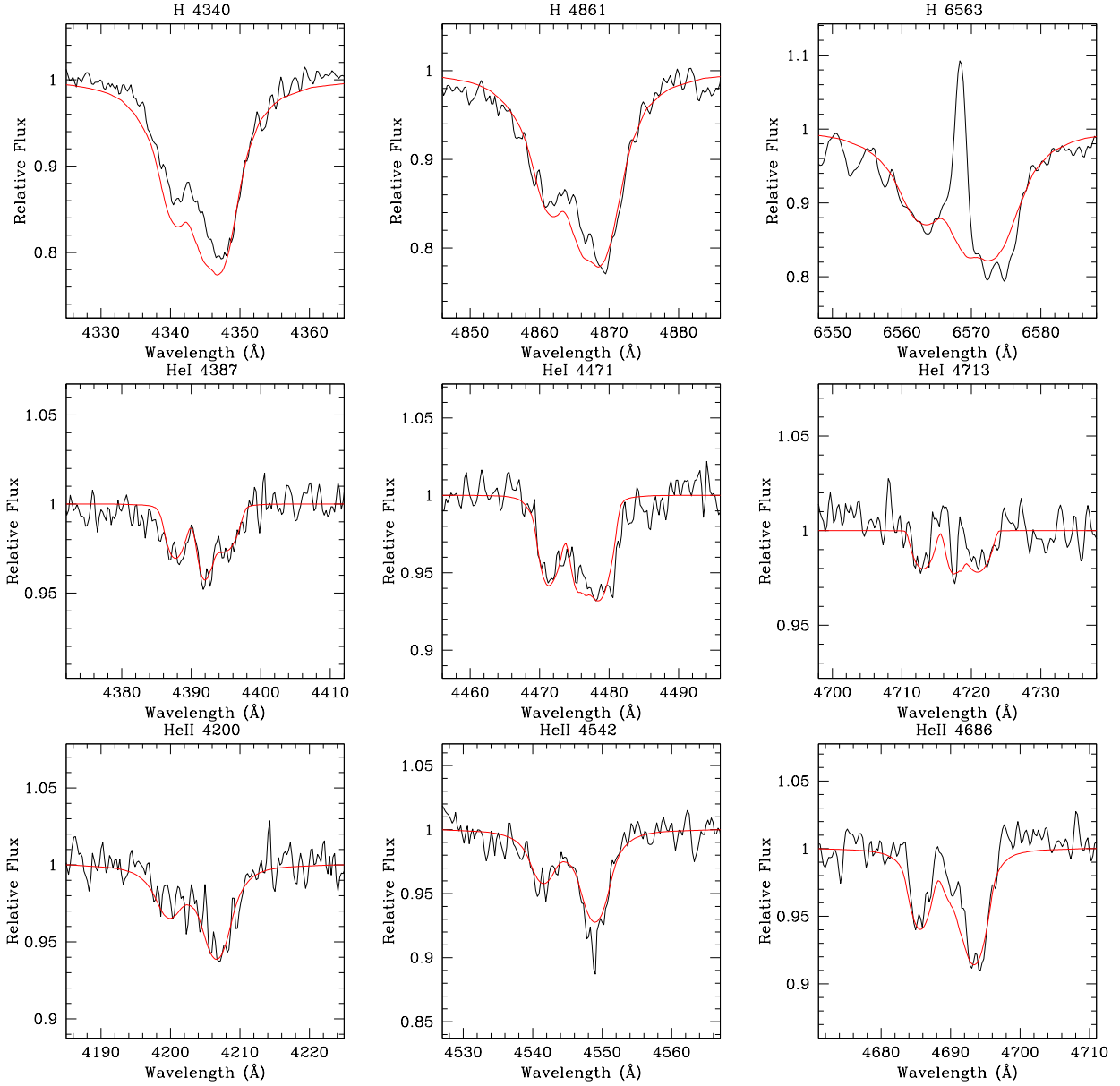


Fig. 10.— LMC ST2-28 comparison with stellar atmosphere models. We compare the combined FASTWIND models (smooth, red curves) with the observed spectrum. The spectrum used was taken on 2454876.697 and corresponds to a phase of 0.702. The top row shows the $H\gamma$, $H\beta$, and $H\alpha$ lines. Note the presence of remaining nebular emission at line center, albeit not as strong as in LMC 172231 (Figure 5). The second row shows the He I λ 4387, He I λ 4922, and He I λ 4713 lines. The bottom row shows the He II λ 4200, He II λ 4542, and He II λ 4686 lines. The latter is primarily sensitive to the mass-loss rate and wind law.

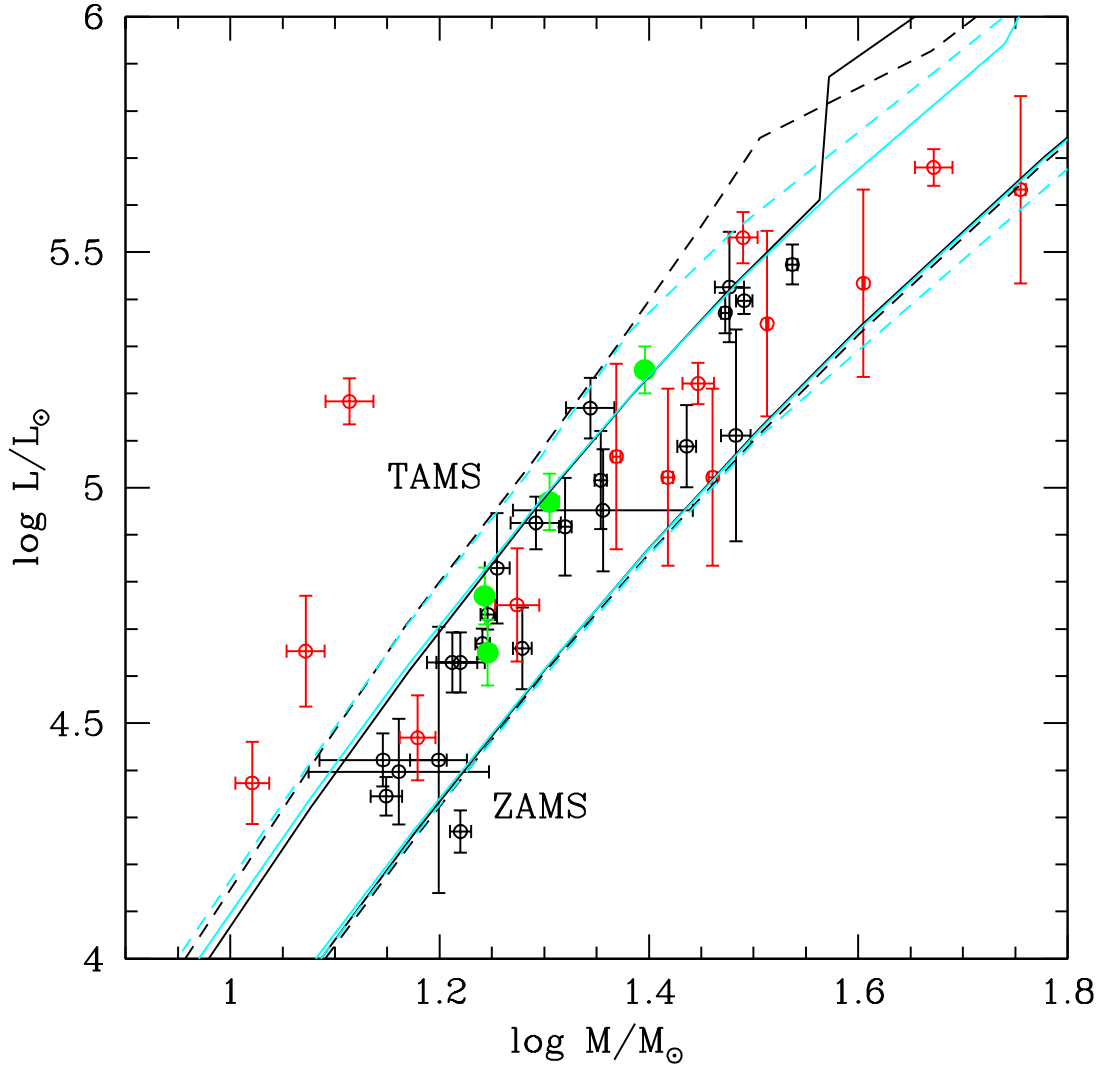


Fig. 11.— The Mass-Luminosity Relationship for massive stars. The colored points are all from LMC binaries, with green presenting the present work, and red representing other data. Black denotes data for Milky Way massive stars. Other than the present work, all the data come from Table 1 in Gies (2012). The three LMC stars whose masses are too low for their luminosities are the secondary component of SC1-105 (Bonanos 2009) and the two components of 78.6097.13 (González et al. 2005). Lines shows the mass-luminosity relationship obtained from the latest Geneva models for solar metallicity (black, Ekström et al. 2011) and for LMC metallicity (cyan, Chomienne et al. 2011, in prep) for the zero-age main-sequence (ZAMS) and terminal-age main-sequence (TAMS). Solid lines denote the mass-luminosity relationship determined from evolutionary models without rotation, while the dashed lines show the theoretical mass-luminosity relationship for models with initial rotation velocities of 40% of the critical velocity.

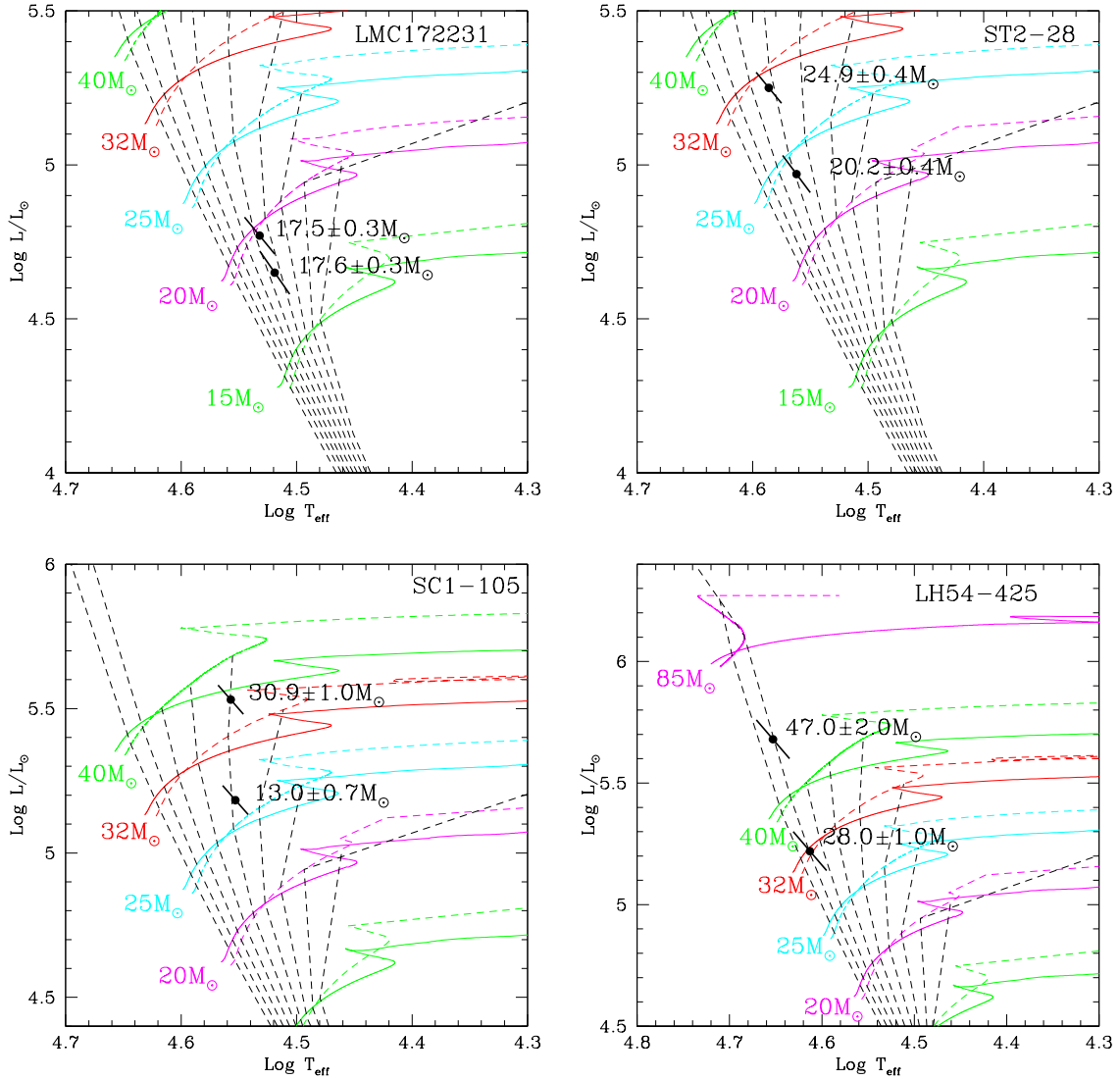


Fig. 12.— Comparison to evolutionary tracks. The location of the stars are indicated in the H-R diagram as points; the associated errors in effective temperatures and luminosities are shown as a diagonal line, as hotter temperatures would lead to higher bolometric luminosity. The new Geneva $z = 0.006$ tracks are shown in colors, with the solid colored lines being the tracks for no rotation, and the dashed colored lines being the tracks computed for an initial rotation of 40% of the critical velocity. The dashed black lines correspond to isochrones of 1-9 Myr at 1 Myr intervals. Note that only the main-sequence, non-WR portion of the tracks (and isochrones) are shown for simplicity. *Upper:* The locations of our stars are shown, labeled with their dynamical masses. *Lower:* The locations of SC1-105 (Bonanos 2009; Bonanos et al. 2011) and LH54-425 (Williams et al. 2008) are shown, also labeled with their dynamical masses.

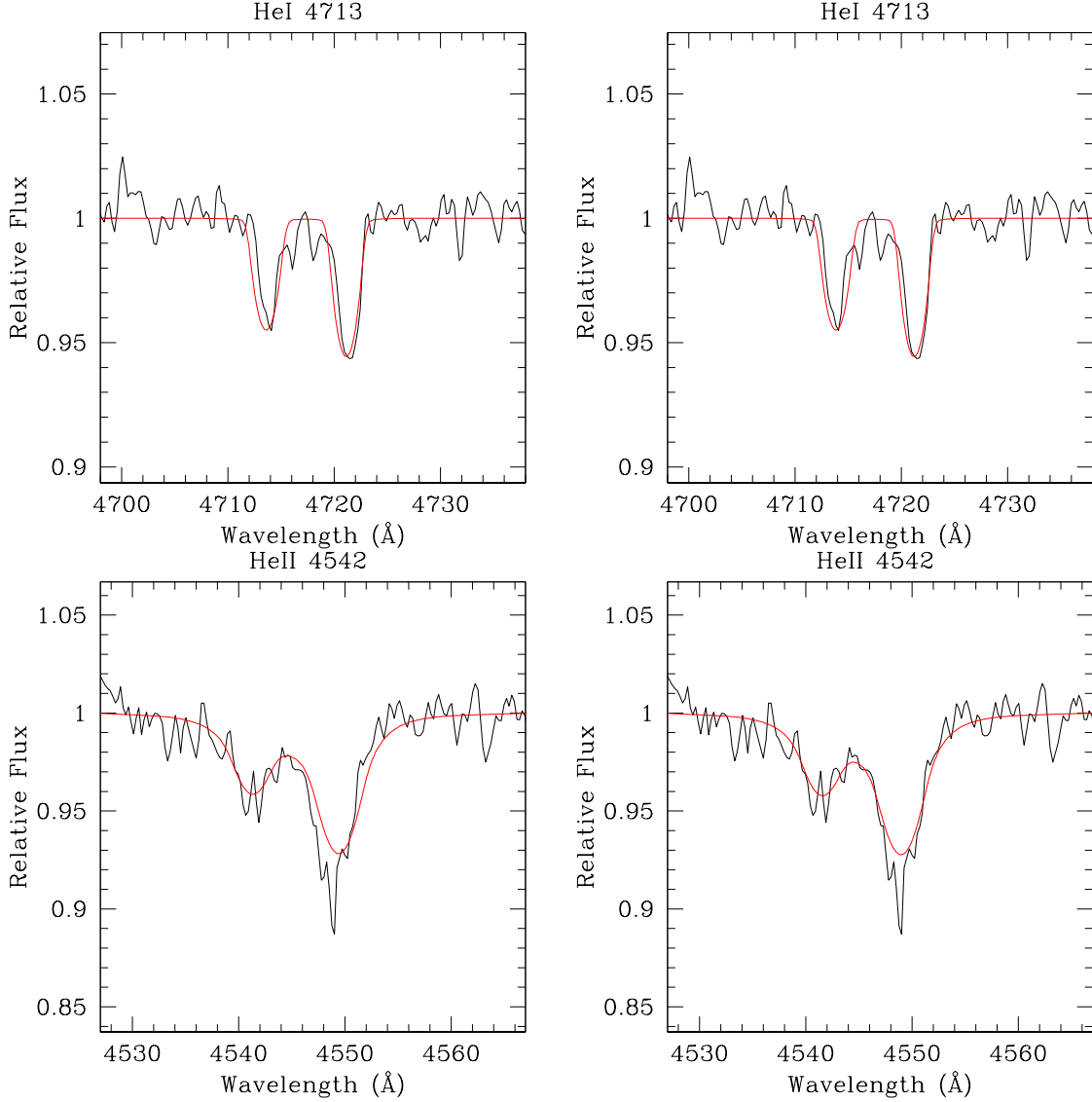


Fig. 13.— Comparison of velocity shifts. *Upper:* The He I $\lambda 4713$ LMC 172331 FASTWIND model lines have been shifted by the amount needed to match the required orbital semi-amplitudes if the evolutionary masses were correct on the left. On the right we show the shifts based upon our adopted orbital semi-amplitudes. The underlying spectrum is that shown in Figure 5. *Lower:* The same is shown for the He II $\lambda 4542$ FASTWIND model lines for ST2-28. The underlying spectrum is that shown in Figure 10.

Table 1. Telescopes Used for Photometry

Index	Telescope	Camera	Observatory	Scale (" / pixel)	FOV	Median (Seeing ("))	# Images
1	Swope 1.0-m	SITe#3	LCO	0.435	15'x23' ^a	1.60	2970
2	SMARTS Yale 1.0-m	Y4KCam	CTIO	0.289	20'x20'	1.67	1836 ^b
3	SMARTS 1.3-m	ANDICAM	CTIO	0.369	6'x6'	1.61	1493 ^b

^aUsually formatted to smaller region.

^bThese include back-to-back exposures, so independent measurements are half of these.

Table 2. Photometric Monitoring of OB Associations^a

Season	NGC 346	NGC 602c	NGC 1910	NGC 2044	NGC 2074	R136
2003/2004	1	1	1
2004/2005	1	1	1	1
2005/2006	2	2	2	2	2	1,2
2006/2007	2	2	2	2	2	2
2007/2008	3	...	3	3	3	3
2008/2009
2009/2010	3	...	3	3	3	3
2010/2011	1,3	1,3	1,3	1,3

^aTelescope/instrument indices from Table 1.

Table 3. Identified Periodic Variables

Star	Ref. ^a	α_{2000}	δ_{2000}	Sp. Type	Period (d)	Status	Comments
SMC NGC 346							
NGC 346 MPG 088	1	00 58 28.41	-72 12 34.3	B2 III	3.61520	Dropped—insufficient spectroscopy	OGLEJ005828.46-721234.1 P=3.615130 ^b
NGC 346 MPG 342	1	00 59 00.01	-72 10 37.8	O5 + O7	2.35482	Dropped—triple lines	
NGC 346 MPG 372	1	00 59 01.88	-72 10 21.3	B 0.2 V ^c	1.19620	Dropped—not double lined	
NGC 346 MPG 644	1	00 59 14.95	-72 11 35.0	B1 V	3.10434	Dropped—insufficient spectroscopy	OGLE SMC-SC8 160725 P=3.104360 ^b
SMC 042367	2	00 58 07.49	-72 15 48.0	B1.5 V	1.41727	Dropped—not double lined	OGLE SMC-SC8 52827 P=1.41713 ^{b,d}
SMC 044626	2	00 58 51.29	-72 05 10.3	B1-2 V	1.52297	Dropped—insufficient spectroscopy	NGC 346 ELS 38
SMC 046456	2	00 59 30.35	-72 09 09.4	B1-2	4.20415	Dropped—not double lined	NGC 346 MPG 782
SMC 047161	2	00 59 46.62	-72 05 32.3	B1 V ^e	3.75305	Dropped—not double lined	NGC 346 ELS 35
NGC 604c							
...		
LMC NGC 1910							
LH41-51	3	05 18 13.81	-69 12 01.2	O9.7 I(f) + O9 V	6.838932	Paper IV	
LH41-52	3	05 18 09.81	-69 11 36.0	B+B	6.55180	Dropped—blended double lines	
LH41-55	3	05 18 25.75	-69 12 12.8	B	1.06203	Dropped—not double lined	
LH41-58	3	05 18 23.75	-69 11 01.5	O8 Iabf + O7 V	4.738649	Paper IV	LMC 110852
LMC NGC 2044							
BAT99-77	4	05 35 59.02	-69 11 47.8	WN7+O3	3.003084	Paper III	HD 269828
Sk -69 ^o 212	5	05 36 06.52	-69 11 47.4	O5 III	2.39929	Dropped—not double lined	
LMC 161594	2	05 34 59.88	-69 16 52.9	Early B	1.64093	Dropped—blended double lines	MACHO 82.8888.31 P=1.64085 ^f
LMC 163970	2	05 35 55.21	-69 08 54.9	O9 V	3.91221	Dropped—blended double lines	MACHO 82.9011.7 P=3.91248 ^f
LMC 164325	2	05 36 02.64	-69 18 21.4	O8 V + O9 V	3.12120	Dropped—blended double lines	MACHO 82.9008.11 P=3.12011 ^f
LMC 164717	2	05 36 10.61	-69 23 09.5	B star	4.77805	Dropped—not double lined	MACHO 82.9128.35 2P=4.77738 ^g
LMC 165507	2	05 36 26.14	-69 19 28.7	M star	1.98748	Dropped—not early-type star	
LMC 165792	2	05 36 32.37	-69 20 51.3	O9.5 I + dwarf	8.10475	Dropped—blended double lines	MACHO 82.9129.7 P=8.09837 ^f
LMC 165885	2	05 36 34.54	-69 15 21.4	B0 V	1.36110	Dropped—not double lined	MACHO 82.9130.20 P=1.36097 ^f
LMC 166580	2	05 36 48.82	-69 16 59.2	B	3.85386	Dropped—blended double lines	MACHO 82.9130.25 P=3.75353 ^h
ST2-28	6	05 35 50.94	-69 12 00.4	O7 V + O8 V	2.762456	This paper	MACHO 82.9010.36 P=2.76245 ^{f,i}
ST2-42	6	05 36 00.01	-69 12 08.6	O8 V + B0 III	4.363011	Paper IV	LMC 164202
ST2-63	6	05 36 11.14	-69 11 01.4	O9	2.43522	Dropped—not double lined	
LMC 169415	2	05 37 51.11	-69 10 59.9	O6 V + O9.5 V	1.777586	Paper IV	
LMC NGC 2074							
LMC 171676	2	05 38 44.88	-69 24 40.1	?	1.25973	Dropped—image multiple	LHA 120-N 158B
LMC 172231	2	05 38 58.23	-69 30 11.4	O9 V + O9.5 V	3.225414	This Paper	[ST92] 5-67
LMC 173064	2	05 39 18.68	-69 28 46.0	B0 III	2.50972	Dropped—not double lined	MACHO 81.9611.8 P=2.50988 ^f
LMC 173712	2	05 39 39.49	-69 29 05.6	O9 III + O9 V	4.912573	Paper IV	MACHO 81.9611.4 P=4.91250 ^{h,j}
W4-6	7	05 39 54.95	-69 24 10.2	O7 III	1.71603	Dropped—not double lined	LMC 174056
Br 95	8	05 40 07.64	-69 24 31.9	WN3 + O7dbl	1.552931	Paper III	HD 269956

Table 3—Continued

Star	Ref. ^a	α_{2000}	δ_{2000}	Sp. Type	Period (d)	Status	Comments
LMC 174250	2	05 40 04.15	-69 27 07.5	B0.7 IV + B1 V	1.483261	Paper IV	MACHO 81.9732.32 P=1.48327 ^f
LMC 174491	2	05 40 14.94	-69 27 58.8	B1 III + B1 IV-V	2.04390	Paper IV	
LMC 174510	2	05 40 15.68	-69 30 28.4	B2 V + B2 V	3.02517	Dropped—blended double lines	MACHO 76.9731.1562 P=3.02596 ^f
LMC 174734	2	05 40 25.14	-69 24 32.7	B0.5 IV + B1 V	2.319493	Paper IV	
LMC R136							
LMC 168477	2	05 37 30.85	-69 05 17.5	O8.5 V + O9 V	2.333363	Paper IV	
LMC 169782	2	05 37 59.57	-69 09 01.4	O4 V + O5 V	1.855280	Paper II	
LMC 171520	2	05 38 41.26	-69 02 58.4	O6 V + O6.5 V	2.875275	Paper II	
R136-015	9	05 38 43.18	-69 05 46.9	O3 If*	4.69880	Dropped—too crowded	
R136-038	9, 10	05 38 42.10	-69 06 07.9	O3 V+ O6 V	3.38845	Dropped—too crowded plus previous orbit	P=3.39 ^k
Mel 50	11	05 38 38.56	-69 06 21.9	O9 I	6.89228	Dropped—blended double lines	
[P93] 467	12	05 38 35.63	-69 06 06.7	O8.5 V	4.27588	Dropped—not double lined, nebular contam.	
[P93] 661	12	05 38 38.81	-69 06 13.2	O4 V	1.58952	Dropped—not double lined	
[P93] 729	12	05 38 39.86	-69 06 08.7	O6-7 dbl	1.58053	Dropped—too crowded	
[P93] 921	12	05 38 42.18	-69 05 45.5	O5 III(f) + O5 V	2.389321	Paper II	
[P93] 1024	12	05 38 43.21	-69 04 13.1	O9 V	4.15991	Dropped—not double lined	Mel 22 ^l
RR Dor	...	05 39 53.32	-69 15 34.7	O9.5 III + B0 III	2.149363	Paper IV	

^aReferences for object identification: 1—Massey et al. 1989; 2—Massey 2002; 3—Lucke 1972; Massey et al. 2000; 4—Breysacher et al. 1999; 5—Sanduleak 1970; 6—Shield & Testor 1992; Massey et al. 2000; 7—Westerlund 1961; 8—Breysacher 1981; 9—Massey & Hunter 1998; 10—Massey et al. 2002; 11—Melnick 1985; 12—Parker 1993

^bWyrzykowski et al. 2004

^cSpectral type from Evans et al. 2006

^dAlso MACHO 207.16490.12 P= 1.41713, from Faccioli et al. 2007 .

^eSpectral type from Hunter et al. 2008

^fDerekas et al. 2007

^gAlcock et al. 1996 quoted in Vizier II/247

^hFaccioli et al. 2007

ⁱAlso LMC 163763

^jPosition of MACHO source differs by 1''7 with ours.

^kMassey et al. 1998

^lMelnick 1985

Table 4. Summary of Light Curve Data

Star	#Data Frames		Time Coverage		Period ^a (days)	θ^b	T ^c
	Raw	Indep. ^d	First	Last			
LMC 172231	544	285	2453591.9	2455618.7	3.225414 (30)	0.07	2453591.469
ST2-28	552	279	2453591.9	2455605.7	2.762456 (10)	0.07	2453590.217

^aThe value in parentheses denotes the uncertainty in the last digits of the period.

^bThe parameter θ is a measure of the reliability of the period derived from the Lafler & Kinman (1965) method, ranging from 0 to 1, with 0 being the most reliable, and 1 having no better significance than random.

^cHJD of primary eclipse.

^dThe number of independent measures, combining the back-to-back photometry into a single value.

Table 5. LMC 172231 Photometry

HJD	V	σ_V	Telescope ^a	Phase ^b
2453606.819	14.040	0.015	2	0.759
2453599.876	14.076	0.015	2	0.607
2453646.710	14.111	0.019	2	0.127
2453679.782	14.090	0.004	2	0.380
2453987.845	14.038	0.008	2	0.892
2453691.714	14.124	0.015	2	0.080
2454061.635	14.029	0.010	2	0.769
2453968.828	14.585	0.013	2	0.995
2453682.720	14.010	0.004	2	0.291
2453643.898	14.079	0.011	2	0.255

Note. — Table 5 is published in its entirety in the electronic edition. A portion is shown here for guidance regarding its form and content.

^aTelescope and instrument combination index as defined in Table 1.

^bBased upon $P = 3.225414$ and $T = 2453591.469$.

Table 6. Radial Velocities LMC 172231

HJD	Phase ^a	v_1	$\sigma_{v_{\text{pri}}}$	v_2	$\sigma_{v_{\text{sec}}}$	# ^b
2454809.842	0.742	455.9	...	30.1	...	1
2454811.595	0.285	47.0	2.4	502.3	7.4	6
2454814.710	0.251	44.0	2.1	512.0	8.8	4
2454877.619	0.755	520.1	3.1	48.4	4.0	10
2455138.693	0.698	452.8	3.2	2.7	3.9	3
2455143.685	0.245	29.1	6.0	479.0	4.8	10
2455143.825	0.289	15.6	1.9	487.1	5.3	10
2455248.576	0.766	519.4	5.5	66.6	2.3	8
2455248.599	0.773	523.7	4.0	62.4	3.8	10
2455249.734	0.125	137.5	6.1	475.1	4.6	10
2455527.606	0.276	30.7	3.1	485.1	5.3	17

^aBased upon $P = 3.225414$ and $T = 2453591.469$.

^bNumber of spectral lines used.

Table 7. Orbital and Physical Parameters LMC 172231

Parameter	Primary	Secondary
Period (days)	3.225414 ± 0.000030	
Time Primary is eclipsed T	2453591.469	
Spectral Types	O9 V	O9.5 V
Orbital Semi-amplitude K (km s^{-1})	234.9 ± 1.7	233.2 ± 1.7
Center of Mass Velocity γ (km s^{-1})	271.5 ± 1.2	
Residuals from fit σ (km s^{-1})	22.6	27.9
$m \sin^3 i$ (M_\odot)	17.1 ± 0.3	17.2 ± 0.3
Orbital inclination i	$83^\circ 0 \pm 0^\circ 5$	
Effective temperature T_{eff}	$34,000 \pm 1,000$	$33,000 \pm 1,000$
Stellar radius R (R_\odot)	7.0 ± 0.3	6.5 ± 0.3
Surface gravity from analysis $\log g$ [cgs]	3.99 ± 0.04	4.06 ± 0.04
Absolute visual magnitude M_V (observed)	-5.0 ± 0.3	
Absolute visual magnitude M_V (total, spherical model)	-4.55 ± 0.05	
Absolute visual magnitude M_V (total, tidal model)	-4.72 ± 0.08	
Visible light flux ratio F_{V_2}/F_{V_1}	0.80 ± 0.03	
Absolute visual magnitude M_V (individual, spherical model)	-3.89 ± 0.07	-3.69 ± 0.07
Absolute visual magnitude M_V (individual, tidal model)	-4.08 ± 0.08	-3.84 ± 0.08
Bolometric luminosity $\log L/L_\odot$ (spherical model)	4.77 ± 0.06	4.65 ± 0.07
Bolometric luminosity $\log L/L_\odot$ (tidal model)	4.84 ± 0.05	4.71 ± 0.05
age ^a t (Myr)	5.2 ± 0.8	5.5 ± 0.5
mass m (M_\odot)	17.5 ± 0.3	17.6 ± 0.3

^aFrom evolutionary models; see text.

Table 8. Comparison of Orbit Solution with Wilson’s Method

Star	Orbit Solution		Wilson’s Method	
	γ	$K_{\text{pri}}/K_{\text{sec}}$	γ	$K_{\text{pri}}/K_{\text{sec}}$
LMC 172231	271.5 ± 1.2	1.01 ± 0.01	269.5 ± 1.9	1.03 ± 0.01
ST2-28	273.8 ± 1.2	0.81 ± 0.01	273.8 ± 2.1	0.81 ± 0.01

Table 9. ST2-28 Photometry

HJD	V	σ_V	Telescope ^a	Phase ^b
2453679.716	14.136	0.009	2	0.398
2453679.734	14.188	0.003	2	0.405
2453691.708	14.245	0.011	2	0.739
2453599.872	14.592	0.013	2	0.495
2453991.844	14.198	0.025	2	0.388
2453600.907	14.210	0.025	2	0.870
2453682.711	14.530	0.007	2	0.482
2453968.825	14.355	0.010	2	0.055
2454061.630	14.153	0.008	2	0.650
2454080.670	14.398	0.011	2	0.542

Note. — Table 9 is published in its entirety in the electronic edition. A portion is shown here for guidance regarding its form and content.

^aTelescope and instrument combination index as defined in Table 1.

^bBased upon $P = 2.762456$ and $T = 2453590.217$.

Table 10. Radial Velocities ST2-28 (He II Lines Only)

HJD	Phase ^a	v_1	$\sigma_{v_{\text{pri}}}$	v_2	$\sigma_{v_{\text{sec}}}$	# ^b
2454810.665	0.798	516.7	1.5	-0.9	1.9	3
2454811.801	0.209	45.1	6.1	554.4	3.1	2
2454813.547	0.842	481.4	4.0	10.4	8.4	2
2454814.557	0.207	38.8	0.8	539.8	9.0	2
2454814.683	0.253	41.5	7.2	568.5	2.6	3
2454814.831	0.306	42.7	10.0	560.5	13.6	2
2454876.697	0.702	499.0	9.8	-14.9	5.8	3
2455136.603	0.787	500.5	...	-17.3	...	1
2455137.798	0.219	44.3	0.2	571.7	11.7	2
2455140.732	0.281	38.6	4.7	568.1	8.0	4
2455141.794	0.666	476.5	5.9	14.0	10.8	4
2455249.601	0.692	499.6	4.3	-13.0	4.2	3
2455249.723	0.736	511.7	5.8	-17.0	8.1	4
2455528.681	0.718	508.6	2.7	-23.2	8.9	4

^aBased upon $P = 2.762456$ and $T = 2453590.217$.

^bNumber of spectral lines used.

Table 11. Orbital and Physical Parameters ST2-28

Parameter	Primary	Secondary
Period (days)	2.762456 ± 0.000010	
Time Primary is eclipsed T	2453590.217	
Spectral Types	O7 V	O8 V
Orbital Semi-amplitude K (km s ⁻¹)	241.0 ± 1.6	297.0 ± 1.9
Center of Mass Velocity γ (km s ⁻¹)	273.8 ± 1.2	
Residuals from fit σ (km s ⁻¹)	6.0	8.6
$m \sin^3 i$ (M_\odot)	24.6 ± 0.3	20.0 ± 0.3
Orbital inclination i	85°0 ± 2°0	
Effective temperature T_{eff}	38,500±1,000	36,500±1,000
Stellar radius R (R_\odot)	9.5 ± 0.3	7.7 ± 0.3
Surface gravity from analysis $\log g$ [cgs]	3.88 ± 0.03	3.97 ± 0.03
Absolute visual magnitude M_V (observed)	-5.5 ± 0.3	
Absolute visual magnitude M_V (total, spherical model)	-5.49 ± 0.10	
Absolute visual magnitude M_V (total, tidal model)	-5.68 ± 0.08	
Absolute visual magnitude M_V (binary only, spherical model)	-5.24 ± 0.04	
Absolute visual magnitude M_V (binary only, tidal model)	-5.44 ± 0.08	
Visible light flux ratio F_{V_2}/F_{V_1}	0.62 ± 0.02	
Third light component $F_{V_3}/(F_{V_1} + F_{V_2})$	0.25 ± 0.10	
Absolute visual magnitude M_V (individual, spherical model)	-4.72 ± 0.05	-4.20 ± 0.06
Absolute visual magnitude M_V (individual, tidal model)	-4.92 ± 0.08	-4.40 ± 0.08
Bolometric luminosity (spherical) $\log L/L_\odot$	5.25 ± 0.05	4.97 ± 0.06
Bolometric luminosity (tidal model) $\log L/L_\odot$	5.33 ± 0.04	5.05 ± 0.05
age ^a t (Myr)	3.6 ± 0.5	4.0 ± 0.5
mass m (M_\odot)	24.9 ± 0.4	20.2 ± 0.4

^aFrom evolutionary models; see text.

Table 12. Comparison with Evolutionary Models

Parameter	Observed	Models	Difference
LMC 172231, $t = 5.3$ Myr			
Mass_{pri}	$17.5 \pm 0.3 M_{\odot}$	$19.6 \pm 0.8 M_{\odot}$	$-2.1 \pm 1.1 M_{\odot}$
Mass_{sec}	$17.6 \pm 0.3 M_{\odot}$	$18.0 \pm 0.8 M_{\odot}$	$-0.4 \pm 1.1 M_{\odot}$
$(\log L/L_{\odot})_{\text{pri}}$	4.77 ± 0.06	4.61 ± 0.02	0.16 ± 0.08
$(\log L/L_{\odot})_{\text{sec}}$	4.65 ± 0.07	4.62 ± 0.02	0.03 ± 0.09
ST2-28, $t = 3.8$ Myr			
Mass_{pri}	$24.9 \pm 0.4 M_{\odot}$	$29.8 \pm 1.2 M_{\odot}$	$-4.9 \pm 1.6 M_{\odot}$
Mass_{sec}	$20.2 \pm 0.4 M_{\odot}$	$24.0 \pm 1.1 M_{\odot}$	$-3.8 \pm 1.5 M_{\odot}$
$(\log L/L_{\odot})_1$	5.25 ± 0.05	5.02 ± 0.02	0.23 ± 0.07
$(\log L/L_{\odot})_2$	4.97 ± 0.06	4.75 ± 0.03	0.22 ± 0.09
LH54-425, $t = 2.0$ Myr			
Mass_{pri}	$47 \pm 2 M_{\odot}$	$50.2 \pm 2.1 M_{\odot}$	-3.2 ± 4.1
Mass_{sec}	$28 \pm 1 M_{\odot}$	$32.2 \pm 1.1 M_{\odot}$	-4.2 ± 2.1
$(\log L/L_{\odot})_{\text{pri}}$	5.68 ± 0.04	5.61 ± 0.05	0.07 ± 0.09
$(\log L/L_{\odot})_{\text{sec}}$	5.22 ± 0.04	5.06 ± 0.03	0.16 ± 0.07